



# Earth's Future

## RESEARCH ARTICLE

10.1029/2024EF004622

### Key Points:

- Future of lake-effect snow storms is explored using Pseudo-Global Warming with a 3D two-way coupled lake-land-atmosphere modeling system
- Future climate amplifies storm precipitation via higher lake evaporation and boosts rainfall at snowfall's expense via a warmer atmosphere
- Lake evaporation plays a critical role in storm precipitation amount and accurately resolving the future lake-atmosphere dynamics is vital

### Supporting Information:

Supporting Information may be found in the online version of this article.

### Correspondence to:

P. Xue,  
pxue@mtu.edu

### Citation:

Kayastha, M. B., Huang, C., Wang, J., Qian, Y., Yang, Z., Chakraborty, T., et al. (2024). How could future climate conditions reshape a devastating lake-effect snow storm? *Earth's Future*, 12, e2024EF004622. <https://doi.org/10.1029/2024EF004622>

Received 28 FEB 2024

Accepted 2 JUN 2024

## How Could Future Climate Conditions Reshape a Devastating Lake-Effect Snow Storm?

Miraj B. Kayastha<sup>1,2</sup> , Chenfu Huang<sup>2</sup>, Jiali Wang<sup>3</sup> , Yun Qian<sup>4</sup> , Zhao Yang<sup>4</sup> , TC Chakraborty<sup>4</sup> , William J. Pringle<sup>3</sup> , Robert D. Hetland<sup>4</sup> , and Pengfei Xue<sup>1,2,3</sup> 

<sup>1</sup>Department of Civil, Environmental, and Geospatial Engineering, Michigan Technological University, Houghton, MI, USA,

<sup>2</sup>Great Lakes Research Center, Michigan Technological University, Houghton, MI, USA, <sup>3</sup>Environmental Science Division, Argonne National Laboratory, Lemont, IL, USA, <sup>4</sup>Pacific Northwest National Laboratory, Richland, WA, USA

**Abstract** Lake-effect snow (LES) storms, characterized by heavy convective precipitation downwind of large lakes, pose significant coastal hazards with severe socioeconomic consequences in vulnerable areas. In this study, we investigate how devastating LES storms could evolve in the future by employing a storyline approach, using the LES storm that occurred over Buffalo, New York, in November 2022 as an example. Using a Pseudo-Global Warming method with a fully three-dimensional two-way coupled lake-land-atmosphere modeling system at a cloud-resolving 4 km resolution, we show a 14% increase in storm precipitation under the end-century warming. This increase in precipitation is accompanied by a transition in the precipitation form from predominantly snowfall to nearly equal parts snowfall and rainfall. Through additional simulations with isolated atmospheric and lake warming, we discerned that the warmer lake contributes to increased storm precipitation through enhanced evaporation while the warmer atmosphere contributes to the increase in the storm's rainfall, at the expense of snowfall. More importantly, this shift from snowfall to rainfall was found to nearly double the area experiencing another winter hazard, Rain-on-Snow. Our study provides a plausible future storyline for the Buffalo LES storm, focusing on understanding the intricate interplay between atmospheric and lake warming in shaping the future dynamics of LES storms. It emphasizes the importance of accurately capturing the changing lake-atmosphere dynamics during LES storms under future warming.

**Plain Language Summary** A lake-effect snow (LES) storm is a heavy snowfall that occurs when a cold dry air mass travels over a relatively warm lake. LES storms have been particularly known to decimate regions downwind of the North American Great Lakes with several meters of snow and millions of dollars in damages. In this study, we use a fully 3D comprehensive lake-land-atmosphere modeling system, along with the Pseudo-Global Warming technique that incorporates large-scale climate changes into our simulation, to investigate how such devastating LES storms could unfold in a warming climate. We used the LES storm that hit Buffalo, New York in November 2022 as a case study. Our results revealed that under a warmer future climate, LES storms can produce a higher precipitation amount by up to 14%. More notably, our results showed a transition in the form of storm precipitation from mostly snowfall to nearly equal parts snowfall and rainfall. The warmer lake in the future was found to be the primary reason behind the increase in precipitation through enhanced evaporation from the lake. The warmer atmosphere in the future explained why rainfall replaced snowfall in the LES storm.

### 1. Introduction

Over the past decades, many weather extremes have escalated in frequency and intensity worldwide, with future projections indicating further increases under climate change (Seneviratne et al., 2021). Extreme weather events were responsible for approximately 475,000 fatalities and trillions of dollars in losses worldwide during 2000–2019 (Eckstein et al., 2021). Consequently, a significant emphasis has been placed on understanding how these extreme events might evolve under future global warming (Seneviratne et al., 2021).

Among the various extreme weather events, lake-effect snow (LES) storm—a meteorological phenomenon characterized by heavy convective precipitation downwind of lakes in the form of snow—is a unique and critical coastal hazard (Ayon et al., 2020; Dewey, 1977; Fujisaki-Manome et al., 2022; Notaro et al., 2013). LES storms are formed when a frigid dry air mass traverses over a substantial stretch of comparatively warmer water, triggering the development of a convective internal boundary layer (Figure 1a). The cooler overlying air mass destabilizes the atmosphere and prompts pronounced vertical heat and moisture flux from the exposed water surface

© 2024, The Author(s).

This is an open access article under the terms of the Creative Commons Attribution License, which permits use, distribution and reproduction in any medium, provided the original work is properly cited.

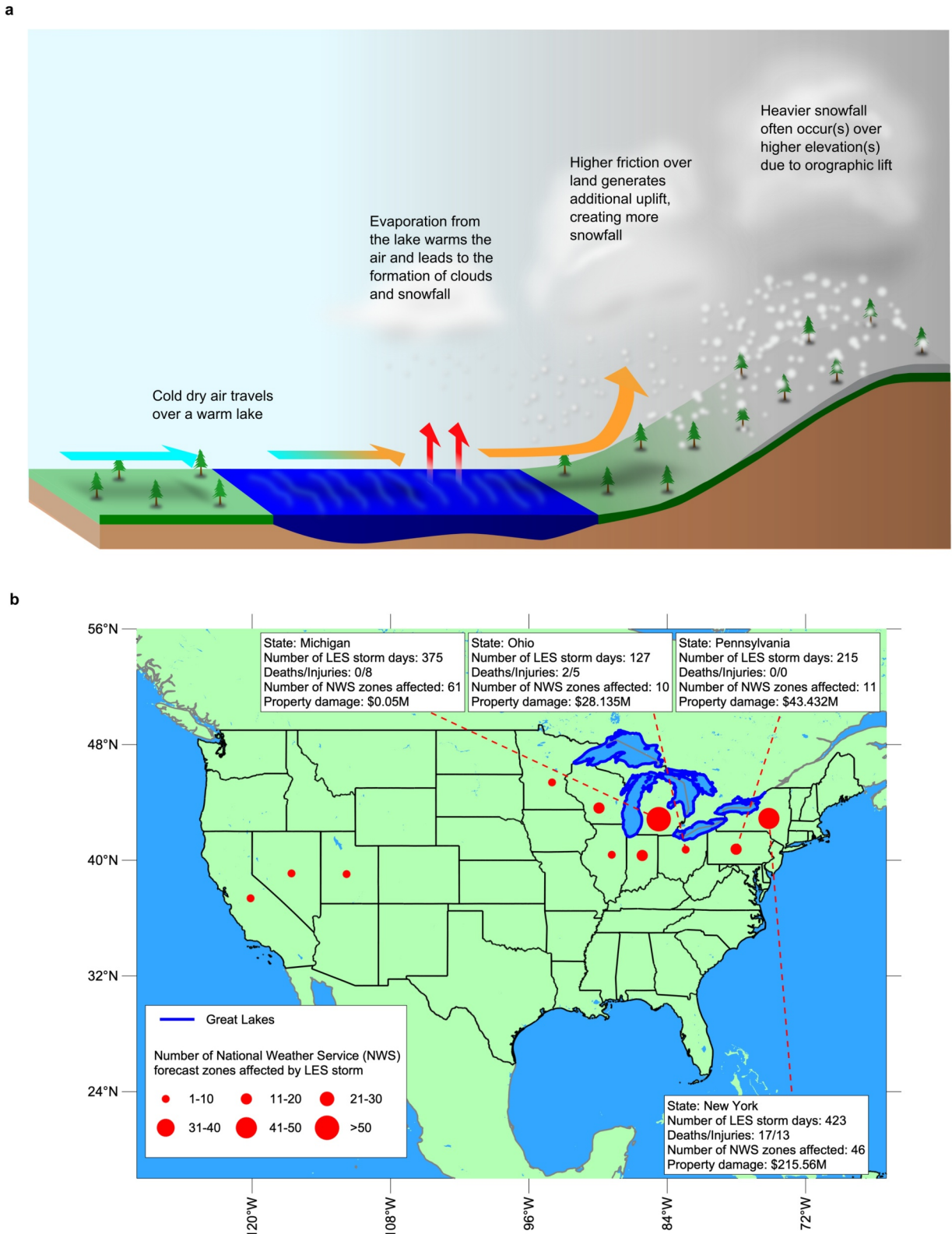


Figure 1.

to the overlying air. This process initiates cloud formation and precipitation, which are further intensified when the moisture-laden air reaches the downwind shores where the land's higher surface roughness relative to the water surface generates an additional uplift of air. Depending on the location, other factors, such as a convergence due to land breezes or an uplift due to orographic effects, also play a role in the intensification of LES storms (Alcott & Steenburgh, 2013; Fujisaki-Manome et al., 2022; Umek & Gohm, 2016; Veals & Steenburgh, 2015).

The world's largest unfrozen surface freshwater system, the Laurentian Great Lakes (Superior, Michigan, Huron, Erie, and Ontario), provides tremendous amounts of moisture that interact with the north-westerly cold dry air, often originating from the Canadian North (Fujisaki-Manome et al., 2022; Notaro et al., 2013; Wright et al., 2013). As such, LES storms play a significant role in shaping the regional Great Lakes climate, especially within the Great Lakes snowbelt, an area of high snowfall along the eastern and southern downwind shorelines. The snowbelt encompasses densely populated regions, including metropolitan cities like Buffalo, New York; Syracuse, New York; Cleveland, Ohio; and London, Ontario. The Canadian snowbelt of Lake Huron alone hosts approximately 1.5 million residents (Bajnath-Rodino & Duguay, 2019). LES storms in the Great Lakes region, therefore, often have extensive societal consequences with multiple human fatalities and injuries, extensive infrastructure damages worth millions of dollars, power disruptions, and hazardous travel conditions (Figure 1b). For this study, LES storms that cause such significant disruption or destruction to human lives and the environment are referred to as devastating LES storms. For instance, in November 1996, a devastating 6-day LES storm near Cleveland dumped nearly 1.75 m of snow and led to eight fatalities, several hundreds of injuries, and economic losses surpassing \$30 million (Kunkel et al., 2002; Schmidlin & Kosarik, 1999). Similarly, an early out-of-season LES storm over Buffalo in October 2006 resulted in 15 fatalities, nearly one million residents without power, \$11 million in disaster grants, and \$150 million in debris removal (NWS, 2006). Two successive LES storms in November 2014 devastated Buffalo once again, producing a combined snow of nearly 3 m and resulting in 13 fatalities and \$46 million in damages (Corcoran et al., 2019; NWS, 2014a, 2014b). Recently, a record-setting LES storm near Buffalo during November 17–20 2022 dumped nearly 2 m of snow and set multiple snowfall records, including both one-day and 2-day snowfall records at county levels (NWS, 2022). With snowfall rates as high as 6 inches per hour over specific locations, the storm decimated the regional infrastructure, with commercial traffic being banned for a 132-mile stretch of the New York State Thruway (Interstate 90) and multiple counties declaring federal emergencies. The storm's property damage alone has been estimated at \$30 million by the National Centers for Environmental Information (NCEI) Storm Event Database (NCEI, 2023).

Such devastating nature of LES storms in the Great Lakes region has motivated multiple studies to improve our understanding of LES by delineating the conditions for LES development (Fujisaki-Manome et al., 2017; Holroyd III, 1971; Welsh et al., 2016; Wiggin, 1950), classifying LES on a synoptic scale (Notaro et al., 2013; Wiley & Mercer, 2020), analyzing the historical trend of LES (Burnett et al., 2003; Suriano & Leathers, 2017), and developing mechanistic lake and atmosphere modeling systems that can more accurately simulate these convective storms (Fujisaki-Manome et al., 2020, 2022; Notaro et al., 2013; Shi & Xue, 2019). By dynamically downscaling Coupled Model Intercomparison Project Phase 5 (CMIP5) Global Climate Models (GCMs), the potential long-term future changes in LES due to climate change have also been examined with findings projecting reduced LES frequency and magnitude, linking them to increases in rainfall at the expense of snowfall (Notaro, Bennington, & Vavrus, 2015). The GCM-driven long-term dynamic downscaling simulations, however, often lack the spatial and temporal resolution needed to capture the fine-scale processes involved in LES storms. They also do not serve the purpose of using extreme historical events to frame plausible future risk to convey complex risk information in a way that is easily understandable by general public (Shepherd et al., 2018).

An alternative approach, known as the storyline approach, is emerging that does not seek to quantify probabilities but instead develops descriptive "storylines" of plausible future climates (Shepherd et al., 2018). The storyline

**Figure 1.** Mechanism behind the manifestation of lake effect snow (LES) storms and an overview of the impact of LES storms in the US. An illustration of the formation of LES storms (a). A map showing the occurrences of LES storms and their impact in different US states (b). The Great Lakes are outlined in dark blue. The red dots represent the occurrences of LES storms while their size represents the number of National Weather Service (NWS) forecast zones affected by the LES storm. The number of LES storm days, deaths, injuries, storm-affected NWS zones, and the magnitude of property damage are provided for four of the most affected states: New York, Pennsylvania, Ohio, and Michigan. Unlike the states bordering the Great Lakes, where LES storms develop due to the Great Lakes, the observations in the three western states correspond to LES storms due to the Great Salt Lake in Utah and Lake Tahoe, which straddles the border of Nevada and California. The state-wise statistics of LES storms were calculated using LES storm data from January 1950 to October 2023, which were obtained from the NCEI Storm Event Database. It should be noted that the property damages statistics come with a disclaimer from NCEI Storm Event Database stating that the property damages should be considered as broad estimates.

approach is a framework used in climate science and risk assessment to explore specific, plausible climate scenarios in detail. Instead of focusing on abstract probabilistic predictions or averages, the storyline approach provides a narrative of how different climate phenomena or weather events could unfold, emphasizing plausible future risks and their potential impacts on specific regions or systems. The main advantage of the storyline approach is that it is narrative-focused for plausible future scenarios, allowing us to use extreme historical events to frame risk in an event-oriented manner. By focusing on particular regions, time frames, or phenomena, it tailors scenarios to specific circumstances. By nature, storylines are not intended for projections, as no *a priori* probability is assessed for a storyline (Shepherd et al., 2018).

A storyline focused on the future of LES storms is a physically self-consistent and plausible event-oriented narrative of a historical LES storm under future climate conditions. Such storylines address a societally relevant question of what will happen to an LES storm if the climate got warmer (Shepherd, 2019) and by doing so, storylines address specific event-related risks that align more closely with the public's perception and response to risks in potentially warmer future climates, particularly for vulnerable areas like Buffalo.

More importantly, it should also be noted that most earlier modeling efforts that investigated the future of LES did not have a robust representation of the future condition of the Great Lakes themselves. LES are manifestations of lake-atmosphere interactions and accurate projections of LES are contingent upon accurate projections of the Great Lakes conditions, particularly lake surface temperature, ice coverage, and the associated moisture and heat fluxes. Yet, the majority of the previous studies derived the Great Lakes conditions from either coarse-resolution GCMs (Suriano & Leathers, 2016) or two-way coupled one-dimensional (1D) lake models (Notaro, Bennington, & Vavrus, 2015). Specifically, GCMs have little to no representation of the Great Lakes (Briley et al., 2021), and 1D lake models struggle to capture the complex three-dimensional (3D) circulation, mixing, and thermal structure of the Great Lakes (Bennington et al., 2014; Kayastha et al., 2023; Xue et al., 2017). Therefore, the Great Lakes communities have recognized a significant need to better explore the future of LES storms through regional climate modeling systems that include a two-way coupled 3D lake model.

This study is the first one to employ the Pseudo-Global Warming (PGW) (Brogli et al., 2023; Schär et al., 1996) method and a regional climate modeling system with a two-way coupled 3D lake model to examine the potential impact of future climate warming on the manifestation and dynamics of LES storms in the Great Lakes region. The PGW method allows for directly assessing what an observed historical event could look like in a different climate and has recently been recommended as the storyline approach for vulnerability assessment (Hazeleger et al., 2015; Shepherd, 2019). PGW simulations are commonly used to investigate a question of the type "How will certain historical or observed events change in a different climate?" and has been widely applied to extreme events including tropical cyclones (Gutmann et al., 2018; Jung & Lackmann, 2019; Patricola & Wehner, 2018), mesoscale convective systems (Haberlie & Ashley, 2019; Prein et al., 2017), atmospheric rivers (Dominguez et al., 2018), and droughts (Ullrich et al., 2018). Using the devastating LES storm that occurred near Buffalo in November 2022 (hereafter referred to as the Buffalo LES storm or simply as the storm) as a demonstration, we provide a storyline with the PGW method on how an LES storm could evolve under a warmer future climate and identify the distinct roles played by the warmer lake and atmosphere conditions.

## 2. Materials and Methods

### 2.1. Study Region

Buffalo is situated within Erie County in the state of New York and is the state's second-most populated city with around 275,000 residents. Located at the downwind eastern tip of Lake Erie (Figure 2), Buffalo is particularly vulnerable to LES storms. The vertical temperature gradient created by the cold air and the warmer Lake Erie, coupled with negligible ice cover, low wind shear, and an extended fetch due to the alignment of prevailing westerly winds with the long axis of the lake, creates favorable conditions for the formation of narrow LES bands that frequently engulf areas in and around Buffalo with devastating LES storms.

### 2.2. Modeling Approach

#### 2.2.1. WRF-FVCOM

A fully 3D two-way coupled lake-land-atmosphere modeling system for the Great Lakes is used to simulate the Buffalo LES storm under the present-day, mid-century, and end-century climates. The modeling system consists

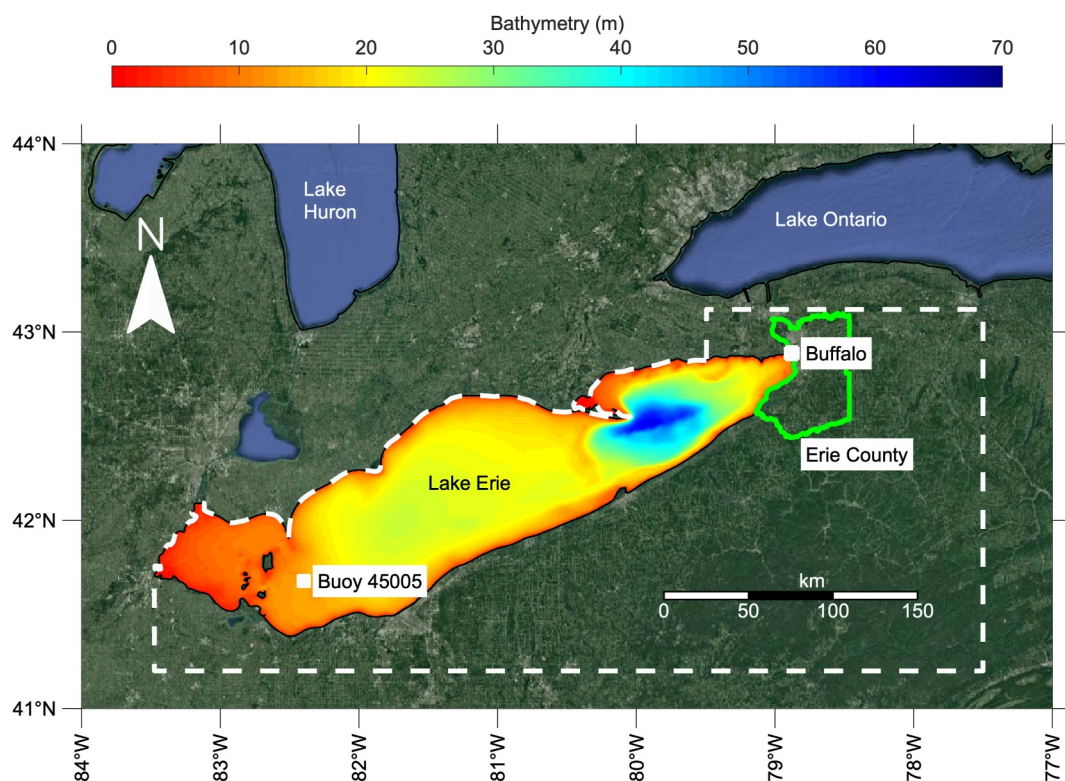


**Figure 2.** Lake Erie and the city of Buffalo. Bathymetric map of Lake Erie, featuring the position of Buoy 45005 of the National Data Buoy Center (NDBC) and the city of Buffalo, which is located within Erie County. The observation data from Buoy 45005 is used for model validation (see Section 2.3. for details). The area enclosed by the white dashed line represents the domain utilized for the atmospheric moisture budget analysis (see Section 2.4. for details).

of the Weather Research and Forecasting (WRF) (Skamarock & Klemp, 2008) model that is two-way coupled to a 3D hydrodynamic lake and ice model based on the Finite Volume Community Ocean Model (FVCOM) (Chen et al., 2006, 2013). This two-way coupled modeling system is referred to as WRF-FVCOM.

WRF-FVCOM uses the WRF model version 4.2.2 with the Advanced Research WRF (ARW) dynamic core to simulate land and atmospheric processes (Skamarock & Klemp, 2008). The WRF domain for this study is centered at 85.0°W, 45.5°N, and encompasses the entire Great Lakes basin with 4 km horizontal grid spacing (Figure S1 in Supporting Information S1). The atmosphere is represented by 50 stretched vertical levels topped at 50 hPa.

The WRF physics selected for this study include the Morrison double-moment microphysics scheme (Morrison et al., 2005), the Rapid Radiative Transfer Model for GCMs longwave and shortwave schemes (Iacono et al., 2008), the Mellor-Yamada-Janjić planetary boundary layer scheme (Janjić, 1994), and the Eta similarity surface layer scheme which is based on the Monin-Obukhov similarity theory (Monin & Obukhov, 1954). The land surface processes are modeled by the Noah-Multiparameterization (Noah-MP) land surface model (Niu et al., 2011). No cumulus parameterizations are used in our WRF setup, as previous studies have demonstrated that a 4 km resolution is adequately convection-permitting in WRF for simulating extreme precipitation (Akinsanola et al., 2024; Kouadio et al., 2020; Qing & Wang, 2021; Sun et al., 2016). Furthermore, our 4 km resolution WRF setup has been used and validated in multiple recent studies for simulating convective precipitation in the Great Lakes region, including Wiley and Mercer (2021), Wang et al. (2022), and Kayastha et al. (2023).

The 3D hydrodynamic lake and ice model within WRF-FVCOM is based on FVCOM model version 4.1, which numerically solves primitive equations over an unstructured triangular grid using the finite volume method in a flux formula and simulates the hydrodynamics, thermal dynamics, and ice dynamics of the Great Lakes. The horizontal resolution of the unstructured triangular grid ranges from ~1 to 2 km near the coast and ~2–4 km in the

**Table 1**  
*Summary of WRF-FVCOM Experiments*

Experiment category	Experiment name	Initial and lateral boundary conditions for WRF	Initial condition for FVCOM	Purpose
I	Case 1	ERA5	Historical standalone FVCOM run	Validate WRF-FVCOM and establish a present-day climate reference for Cases 2, 3, and 4
II	Case 2a	PGW (mid-century)	GLARM (mid-century)	Simulate the Buffalo LES storm under a warmer future climate
	Case 2b	PGW (end-century)	GLARM (end-century)	
III	Case 3a	PGW (mid-century)	Historical standalone FVCOM run	Isolate the impact of a warmer future atmosphere on the Buffalo LES storm
	Case 3b	PGW (end-century)	Historical standalone FVCOM run	
IV	Case 4a	ERA5	GLARM (mid-century)	Isolate the impact of a warmer future lake on the Buffalo LES storm
	Case 4b	ERA5	GLARM (end-century)	

*Note.* All experiments include 10 WRF-FVCOM simulations, each with a different initial condition. In total, 70 WRF-FVCOM simulations were conducted.

offshore region, thereby resolving the complexity of the Great Lakes coastline (Figure S1 in Supporting Information S1). The lakes are vertically represented by 40 sigma layers in FVCOM to provide a vertical resolution ranging from <1 m in nearshore waters to ~2–5 m in the lake's offshore regions. Such a high vertical resolution allows FVCOM to capture the abrupt changes in Great Lakes bathymetry as well. Vertical mixing processes are simulated with the Mellor–Yamada level-2.5 (MY25) turbulence closure model (Mellor & Yamada, 1982), and horizontal diffusivity is computed using the Smagorinsky numerical formulation (Smagorinsky, 1963). An unstructured-grid version of the Los Alamos Community Ice Code (CICE) (Anderson et al., 2018), which is integrated within the FVCOM framework, was used to simulate the ice dynamics, ice thermal dynamics, and ice-water interaction processes of the Great Lakes.

In the two-way coupled framework of WRF-FVCOM, WRF and FVCOM are run simultaneously with a two-way information exchange at 1-hr intervals using the OASIS3-MCT coupler (Craig et al., 2017). During the exchange, FVCOM dynamically calculates the LST and ice cover of the Great Lakes and provides them to WRF as the lower boundary conditions for the atmosphere over the Great Lakes. In turn, WRF dynamically calculates and provides the atmospheric forcings required by FVCOM. The atmospheric forcings include air temperature, air pressure, relative and specific humidities, total cloud cover, wind speed, downward shortwave radiation, and downward longwave radiation. Additionally, in line with Xue et al. (2022), the FVCOM variant used in this study avoids any nudging or other non-physical constraints, thus enabling the Great Lakes hydrodynamics to freely interact with the overlying atmospheric conditions during the simulation. A two-way coupled 3D representation of the Great Lakes within regional climate modeling systems using FVCOM, as employed in this study, has been effectively utilized in previous research as well (Kayastha et al., 2022, 2023; Sun et al., 2020; Xue et al., 2017, 2022).

### 2.2.2. Numerical Experiments

This study involves seven WRF-FVCOM experiments, which are grouped into four different experiment categories (Table 1).

Category I of WRF-FVCOM experiments involves an experiment named Case 1, which simulates the storm under the present-day climate. Case 1 was performed to evaluate WRF-FVCOM's ability to reproduce the observed condition of the storm, while also serving as the reference condition for comparison with other experiments.

In Case 1, the initial and lateral boundary conditions for WRF to dynamically downscale were from the 3-hourly 0.25° fifth-generation atmospheric reanalysis data (ERA5) (Hersbach et al., 2020) of the European Centre for Medium-Range Weather Forecasts (ECMWF). No boundary nudging was applied so WRF-FVCOM was allowed to develop its own variability (e.g., spatial and internal variability) across the domain. Additionally, the initial lake conditions for WRF-FVCOM were derived from the outputs of a separate 5-year (2017–2022) continuous standalone FVCOM spinup driven by the High-Resolution Rapid Refresh (HRRR) (Benjamin et al., 2016) data

from the National Oceanic and Atmospheric Administration (NOAA). This approach facilitated the establishment of appropriate initial conditions at each grid and vertical layer within FVCOM.

Category II of WRF-FVCOM experiments involves developing the future storylines of the storm by simulating the storm under a warmer future climate. More specifically, experiments Case 2a and Case 2b were performed to examine how the storm could unfold under the warmer climates of mid-century and end-century, respectively. These two experiments, which are collectively referred to as Case 2, were carried out through the PGW method, which involves imposing large-scale mean climate change signals in the thermodynamic structure onto the present-day climate. Specifically, the mean climate change signals from 11 Coupled Model Intercomparison Project Phase 6 (CMIP6) GCMs (Table S1 in Supporting Information S1) were superimposed onto the corresponding 3-hourly ERA5 variables to generate the WRF initial and lateral boundary conditions for Case 2. The perturbed variables included the 3D fields of air temperature, specific humidity, geopotential height, as well as surface pressure, sea-level pressure, and skin temperature. The mean climate change signals for Case 2a and Case 2b were computed by comparing the historical period (1981–2010) with the mid-century (2031–2060) and the end-century (2071–2100) periods, respectively. The Shared Socioeconomic Pathway 5 (SSP5-8.5) was considered in Case 2a and Case 2b as it represents the higher end of the spectrum of plausible future pathways and closely corresponds to the Representative Concentration Pathway (RCP) 8.5 (Meinshausen et al., 2020; Riahi et al., 2011).

Meanwhile, to ensure that the lake conditions accurately reflect a warmer climate, the initial lake conditions for WRF-FVCOM simulation in Case 2a and Case 2b were derived by perturbing the initial conditions for FVCOM in Case 1 with climate change signals in lake thermal structure, projected from the Great Lakes-Atmosphere Regional Model (GLARM) (Xue et al., 2017, 2022). Similar to WRF-FVCOM, GLARM is a fully 3D two-way coupled modeling system that couples the fourth version of the International Centre for Theoretical Physics (ICTP) Regional Climate Model (RegCM4) (Giorgi et al., 2012) and FVCOM to represent the Great Lakes system. It has been extensively validated and utilized to project the long-term climate of the Great Lakes region (Kayastha et al., 2022; Xue et al., 2022). In this study, the climate change signals from GLARM consisted of the future changes under RCP 8.5 in ice cover and lake temperature at each grid and vertical layer of FVCOM. These climate change signals were computed by comparing the historical period (1981–2010) with the mid-century (2031–2060) and the end-century (2071–2100) periods. Utilizing the climate change signal for every vertical layer from GLARM ensures that the entire lake column accurately reflects the conditions of a warmer climate. This approach is necessary because if only the lake surface is subjected to future warming, the warming signal at the lake surface would quickly dissipate due to mixing within the lake.

Category III of WRF-FVCOM experiments investigates the impact of atmospheric warming on the storm. Specifically, two experiments named Case 3a and Case 3b were conducted to isolate the response of the storm to the warmer atmospheres of mid-century and end-century, respectively. In Cases 3a and 3b, which are collectively referred to as Case 3, only the initial and lateral boundary conditions for WRF were modified using the PGW method from Case 2.

Category IV of WRF-FVCOM experiments investigates the impact of lake warming on the storm. Two experiments named Case 4a and Case 4b were conducted to isolate the response of the storm to the warmer lake of mid-century and end-century, respectively. In these two experiments, which are collectively referred to as Case 4, only the initial conditions for FVCOM were modified using the GLARM climate change signals from Case 2. The results from Cases 3 and 4, collectively, provide a mechanistic understanding of the results from Case 2, in which both the atmosphere and lake are warmed to future conditions.

In each of the seven experiments from Category I to IV, an ensemble of 10 simulations was performed. Each ensemble member was initialized at a different time to consider the uncertainties from internal variability by allowing each ensemble member to realize its own natural variability. The initialization times were at 12-hr intervals, starting from 00:00 UTC on November 10 to 12:00 UTC on 14 November 2022. Regardless of the initialization time, all the simulations end at 00:00 UTC on 22 November 2022.

### 2.3. Data for WRF-FVCOM Validation

The precipitation from WRF-FVCOM was evaluated against the Stage IV (Du, 2011) data set developed by the National Centers for Environmental Prediction (NCEP), the Precipitation-Elevation Regressions on Independent

Slopes Model (PRISM) (Daly et al., 1994, 2008) data set, and the Snow Data Assimilation System (SNODAS) data set developed by the National Operational Hydrologic Remote Sensing Center (NOHRSC). In addition to precipitation, the simulated rainfall, snowfall, snow water equivalent (SWE), and snow depth were validated against those from SNODAS while the simulated overland air temperature was validated against the temperature from PRISM. The simulated SWE and snow depth were also compared against the SWE and snow depth data set developed by the University of Arizona (Broxton et al., 2019), which is hereafter referred to as the UA data set.

NCEP's Stage IV provides hourly precipitation over the contiguous United States (CONUS) on a 4 km resolution grid by mosaicking the multi-sensor analyses produced by the 12 River Forecast Centers (RFCs) in CONUS. Stage IV blends both observation data and radar-calculated reflectivity, thereby leveraging the accuracy of ground truth from gauges and the spatial comprehensiveness of radar data.

PRISM provides daily precipitation and air temperature over CONUS at a spatial resolution of 4 km. PRISM uses a digital elevation map and ~13,000 weather station data from multiple sources to interpolate and create the gridded precipitation map. PRISM values undergo correction for systematic elevation effects through a climate-elevation regression approach that incorporates weighted station data, with the weights determined based on the station's physiographic characteristics. It should be noted that PRISM defines a day as 1200 UTC - 1200 UTC and uses the day-ending naming convention (e.g., a day ending at 1200 UTC on 1 March is labeled 1 March). This convention has been considered when comparing WRF-FVCOM against the daily PRISM precipitation and air temperature.

SNODAS, on the other hand, caters more toward snow-related variables because its development was geared toward providing the best possible estimates of snow cover and associated parameters to aid hydrologic modeling and analysis. SNODAS provides daily rainfall, snowfall, SWE, and snow depth on a 1 km resolution grid over a domain that encompasses CONUS. To validate WRF-FVCOM's precipitation, the rainfall and snowfall from SNODAS were summed up to obtain the SNODAS's precipitation estimate. SNODAS is a modeling and data assimilation system that downscals the output from the numerical weather prediction (NWP) models and uses a physically based snow model to simulate snow cover. SNODAS assimilates satellite-derived, airborne, and ground-based observations of snow-covered areas and SWE. Similar to PRISM, SNODAS employs a unique definition of a day, which has been considered when comparing WRF-FVCOM against SNODAS. For daily total rainfall and snowfall, SNODAS defines a day from 0600 UTC - 0600 UTC and uses the day-ending naming convention.

The UA data set provides a spatial coverage of daily SWE and snow depth at a spatial resolution of 4 km over CONUS. The development of UA involves combining in situ measurements of SWE from the Natural Resource Conservation Service Snowpack Telemetry (SNOWTELE) network and in situ measurements of snow depth from the National Weather Service Cooperative Observer Program (COOP) network with the temperature and precipitation from PRISM. At the time of writing, UA only has data until September 2021, so we employed the provisional UA data to validate WRF-FVCOM.

The simulated LST from WRF-FVCOM was compared against observations from an NDBC buoy located in the western basin of Lake Erie (Figure 2) and from the Great Lakes Surface Environmental Analysis (GLSEA) (Schwab et al., 1999) data set which was developed by the NOAA Great Lakes Environmental Research Laboratory (GLERL). GLSEA is considered to be one of the most accurate LST data sets for the Great Lakes with a horizontal spatial resolution of 1.3 km. The GLSEA LST are generated using cloud-free portions of satellite images from the NOAA Advanced Very High Resolution Radar (AVHRR) and the Visible Infrared Imaging Radiometer Suite onboard the Suomi National Polar-Orbiting Partnership spacecraft (VIIRS S-NPP) and the NOAA-20 spacecraft (VIIRS NOAA-20).

Similar to LST, the simulated overlake air temperature was compared against observations from an NDBC buoy in Lake Erie's western basin (Figure 2). This comparison was necessitated because PRISM does not provide overlake air temperature over the Great Lakes.

#### 2.4. Computation of Moisture Source's Contribution to Storm Precipitation

To investigate the changes in LES storm from a moisture budget perspective, the contributions of moisture sources for the storm precipitation were calculated using the atmospheric moisture budget equation (Fujisaki-Manome et al., 2017; Yang et al., 2019), which describes the change in the precipitable water ( $PW$ ) as a function

of land evapotranspiration ( $ET$ ), lake evaporation ( $E$ ), precipitation ( $P$ ), and vertically-integrated moisture flux divergence ( $VIMFD$ ). The atmospheric moisture budget equation is as follows:

$$\int Pdt = \int Edt + \int ETdt - \Delta PW - \int VIMFDdt$$

where  $\int Pdt$  is cumulative precipitation,  $\int Edt$  is cumulative evaporation from Lake Erie,  $\int ETdt$  is cumulative evapotranspiration from land,  $\Delta PW$  is the change in precipitable water, and  $\int VIMFDdt$  is cumulative vertically-integrated moisture flux divergence.

$PW$  and  $VIMFD$  were calculated using the following:

$$PW = \frac{1}{g} \int_{Pt}^{Ps} qdp$$

$$VIMFD = \frac{1}{g} \nabla \cdot \int_{Pt}^{Ps} V \cdot qdp$$

where  $q$  is specific humidity,  $g$  is the acceleration due to gravity,  $V$  is the horizontal wind,  $Pt$  is the air pressure at the top of the atmosphere, and  $Ps$  is the surface air pressure.

The cumulative components were calculated from 0000 UTC on November 15 to 1200 UTC on November 21. The spatial domain over which the moisture budget components were calculated is represented by the dashed white line in Figure 2. This domain encompasses the downwind section of Lake Erie and closely resembles the domain used by Fujisaki-Manome et al. (2017) in their atmospheric moisture budget analysis of the November 2014 Buffalo LES storm.

## 2.5. Computation of Rain-On-Snow (ROS) Intensity

To investigate the potential impact of changing LES storm on other concurrent winter hazards amid climate change, we analyzed the Rain-on-Snow (ROS) event (McCabe et al., 2007; Musselman et al., 2018) during the Buffalo LES storm. ROS events are defined as rainfall of at least 3 mm/day falling on a snowpack of at least 10 mm SWE, where the snowmelt makes up at least 20% of the sum of rainfall and snowmelt. The ROS events were identified on a daily scale during November 16–20 for each grid point. The snowmelt for a day was calculated by subtracting the day's SWE from the next day's SWE. These ROS criteria have been adopted in prior studies to identify ROS days that have flood-generating potential in various locations including the coterminous US (Li et al., 2019) and central Europe (Freudiger et al., 2014).

## 3. Results

### 3.1. WRF-FVCOM Validation

The total precipitation, snowfall, and rainfall during November 16 to 21 from WRF-FVCOM is validated against SNODAS (Figure 3). The highest total precipitation was observed over the southeastern shore of Lake Erie and WRF-FVCOM captures this spatial pattern. The north and eastward extent of the storm is slightly smaller in WRF-FVCOM but the highly storm-impacted area is consistently within Erie County in both WRF-FVCOM and SNODAS. In the highly storm-affected region near the southern part of Erie County, WRF-FVCOM simulates a total precipitation of around 140 mm which is slightly higher than the total precipitation from SNODAS of around 115 mm. Most of the storm precipitation is in the form of snow and this composition of precipitation is well reproduced by WRF-FVCOM. It should be noted that the units for precipitation and its components, snowfall and rainfall, are presented in millimeters (mm) of equivalent liquid water for consistency. Snow depth, on the other hand, is presented as the depth of accumulated snow on the ground.

WRF-FVCOM not only accurately captures the total precipitation and snowfall, but also accurately resolves the temporal evolution of precipitation, snowfall, and rainfall over Erie County (Figures 4a–4e). The storm's temporal

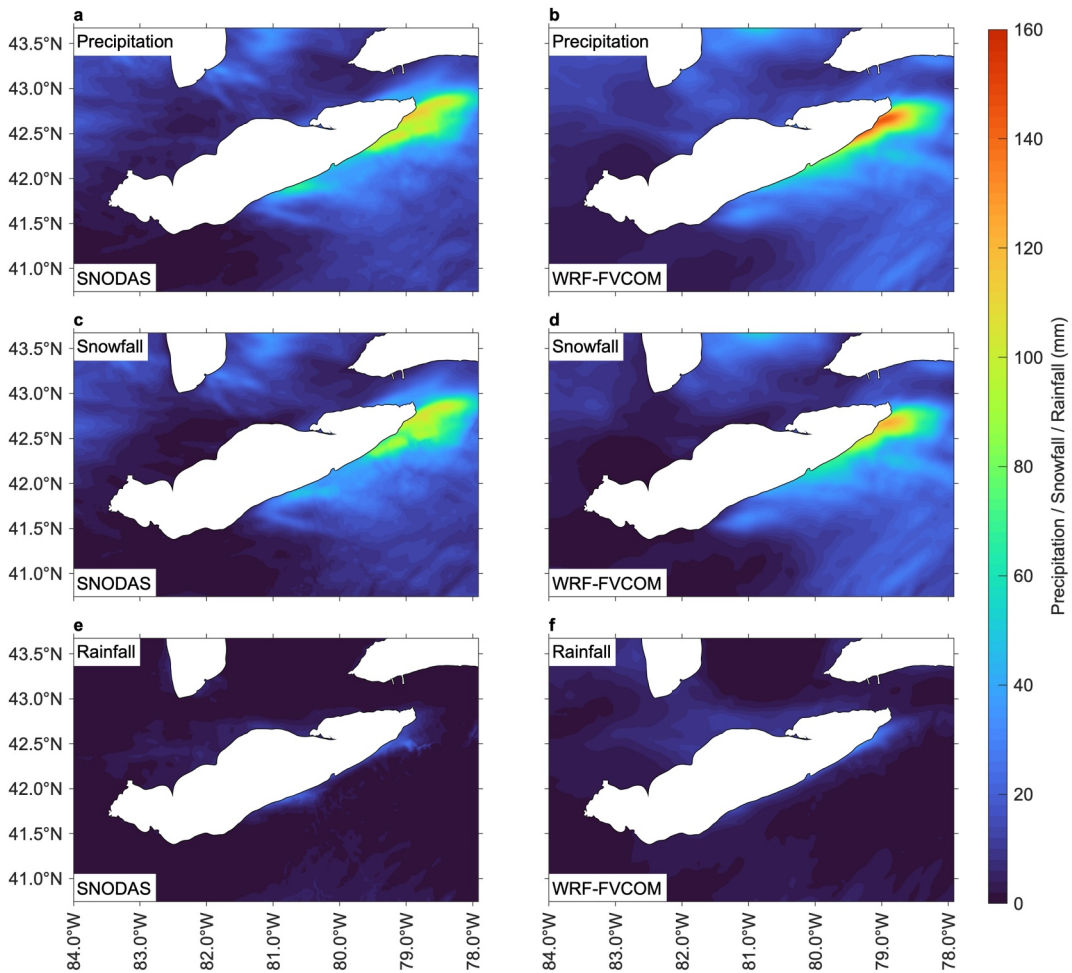


**Figure 3.** Model-observation comparison for storm totals. Total precipitation (a, b), total snowfall (c, d), and total rainfall (e, f) during November 16–21, 2022 from SNODAS and WRF-FVCOM. The results for WRF-FVCOM are the WRF-FVCOM's 10-member ensemble mean.

evolution from WRF-FVCOM is compared against Stage IV, SNODAS, and PRISM. WRF-FVCOM reproduces the hourly precipitation from StageIV over Erie County very well with a correlation of 0.82 and a root mean square error (RMSE) of 0.40 mm. WRF-FVCOM successfully captures the precipitation spikes observed at 2300 UTC on 16 November 2100 UTC on November 18, and 0400 UTC on November 20. WRF-FVCOM does, however, produce a precipitation spike of around 3 mm at 0300 UTC on November 18 which is not observed in Stage IV. Since WRF-FVCOM's hourly precipitation is comparable to observation, WRF-FVCOM's daily precipitation is also comparable to both PRISM and SNODAS, regardless of the different day definitions used in PRISM and SNODAS. This is demonstrated by the excellent performance of WRF-FVCOM in validating daily precipitation against PRISM and SNODAS, with a remarkably high correlation ( $\geq 0.97$ ) and low RMSE ( $\leq 2.63$  mm). Additionally, since most of the precipitation is in the form of snow, the evolution of snowfall over Erie County from SNODAS is also well reproduced in WRF-FVCOM with a correlation of 0.99 and RMSE of 3.17 mm. Average rainfall is also well tracked in WRF-FVCOM although the rainfall during peak precipitation (November 19) is slightly overestimated by around 2 mm.

The evolution of average SWE and snow depth over Erie County from WRF-FVCOM is compared against SNODAS and UA (Figures 4f and 4g). WRF-FVCOM effectively tracks both SWE and snow depth, exhibiting a strong correlation with observations ( $\geq 0.99$ ). However, it is noted that SWE and snow depth from WRF-FVCOM are significantly closer to the values from UA than SNODAS, which highlights the uncertainties in the observation data sets. The RMSE against UA is 2.44 mm for SWE and 36.17 mm for snow depth, while the RMSE against SNODAS is 14.11 mm for SWE and 78.13 mm for snow depth. Compared to SNODAS, both WRF-

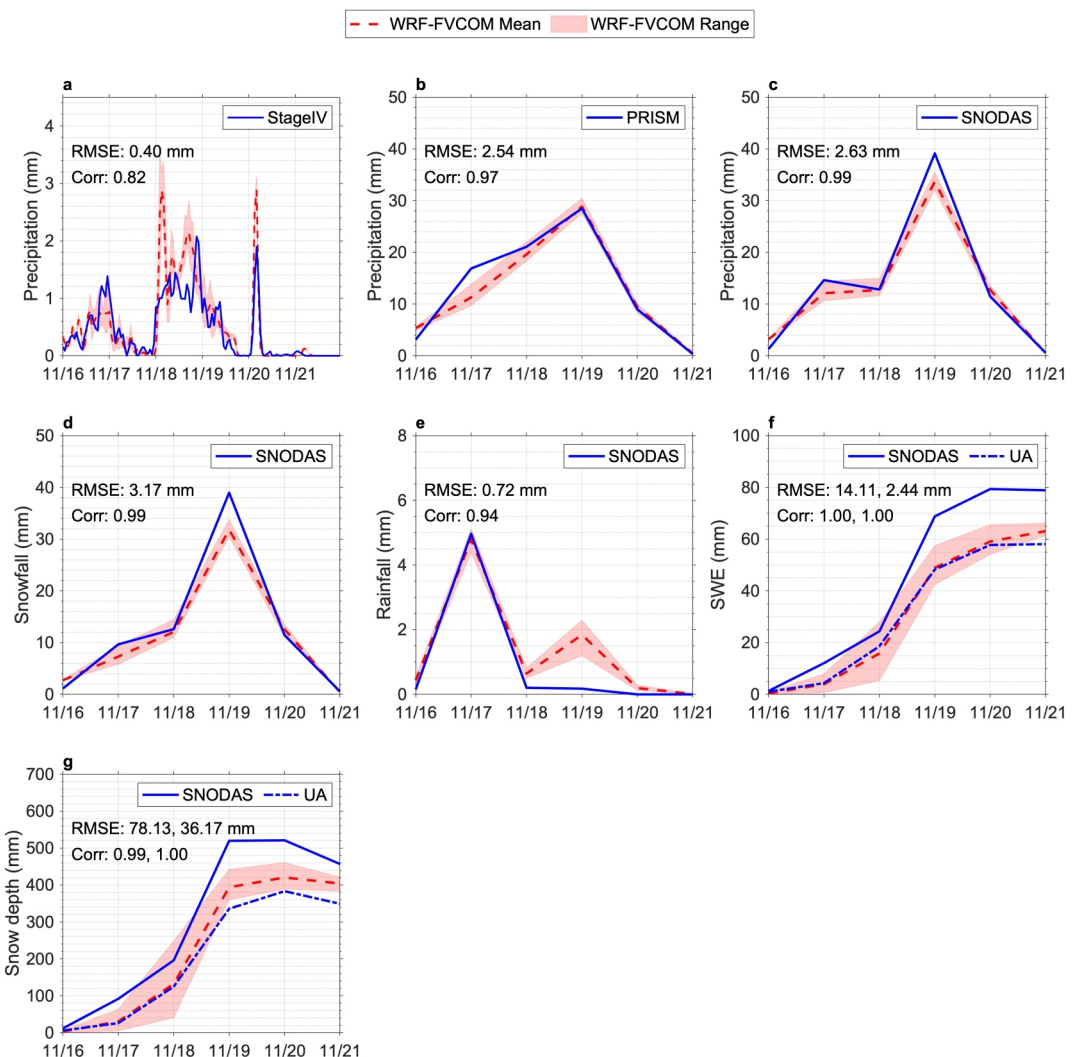


**Figure 4.** Model-observation comparison for temporal storm evolution. Hourly precipitation (a), daily precipitation (b, c), daily snowfall (d), daily rainfall (e), daily SWE (f), and daily snow depth (g). The values are averaged over Erie County and the WRF-FVCOM 10-member ensemble mean is in red while the values from the various observation data sets are in blue. The range of the WRF-FVCOM ensemble is shown by the red shading.

FVCOM and UA tend to estimate a lower SWE and snow depth; but the overall trend of SWE and snow depth during the storm is well simulated by WRF-FVCOM.

Since the majority of the precipitation during the storm is in the form of snow, it is important to evaluate the spatial evolution of WRF-FVCOM's snowfall and SWE against observations like SNODAS (Figure 5). WRF-FVCOM performs well in reproducing the LES band initiation, intensification, and decay. The LES band forms on November 17 over the southeastern shore of Lake Erie and weakens slightly during November 18 after which it peaks on November 19. The LES band then starts to decay as it shifts northward on November 20 and fully diminishes by November 21. The spatial coverage of the LES band over land is marginally smaller in WRF-FVCOM, leading to a narrower spatial extent of SWE compared to SNODAS. Nevertheless, WRF-FVCOM successfully reproduces the persistent high SWE observed in the southeastern shores from November 19–21 and effectively captures the overall spatial progression of both snowfall and SWE.

For air temperature over land, validation was performed over the US as PRISM does not cover the Great Lakes and Canada (Figures 6a and 6b). The longitudinal gradient in overland air temperature with cooler eastern shores is well reproduced by WRF-FVCOM, albeit with a moderate cold bias of  $2^{\circ}\text{C}$ . The evolution of air temperature is also accurately captured by WRF-FVCOM with high correlation ( $\geq 0.96$ ) and low RMSE ( $\leq 2.03^{\circ}\text{C}$ ) (Figure 6c).

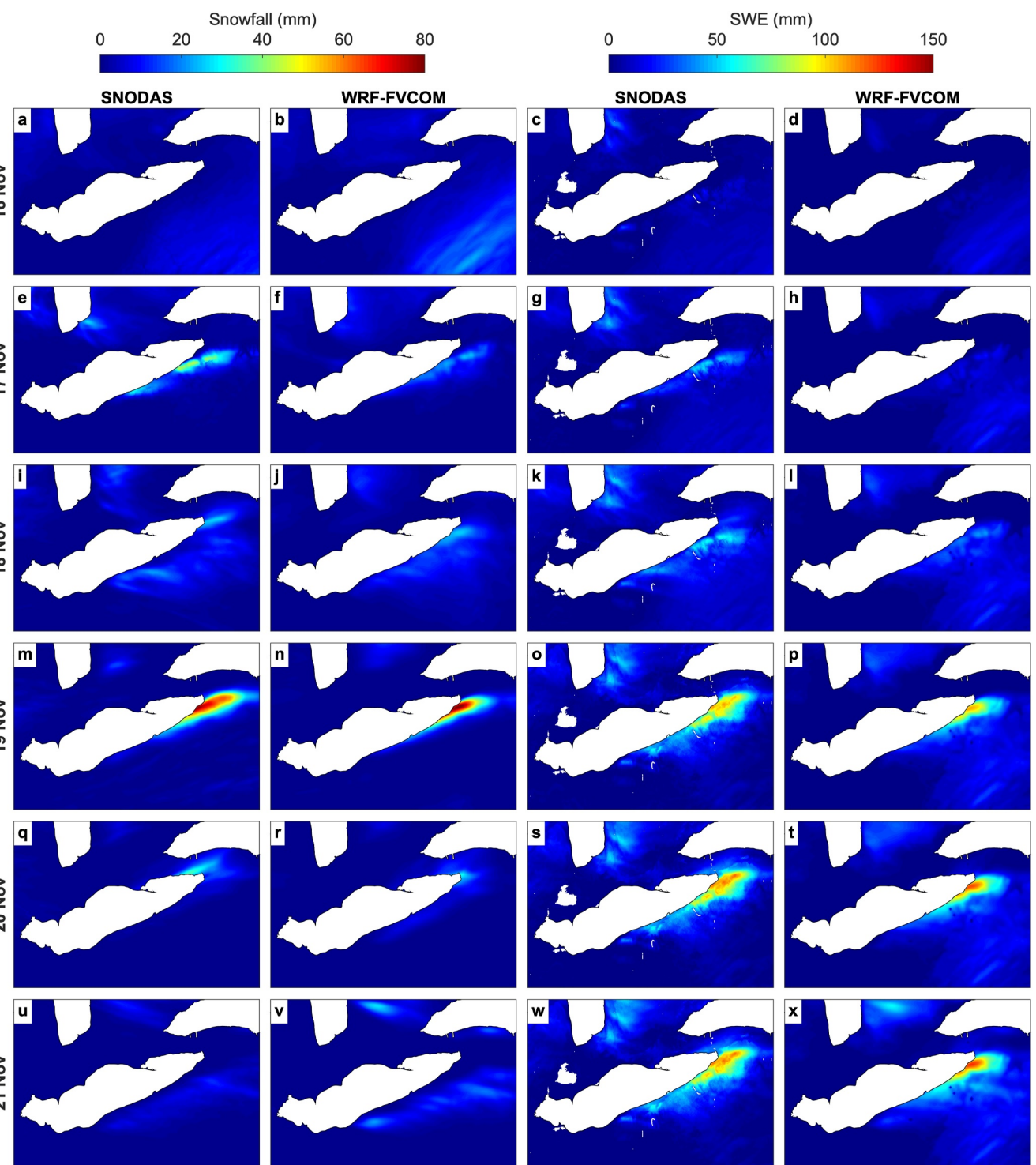


**Figure 5.** Model-observation comparison for spatial evolution of snowfall and SWE. Daily snowfall and daily SWE for November 16 (a–d), November 17 (e–h), November 18 (i–l), November 19 (m–p), November 20 (q–t), and November 21 (u–x). The values for WRF-FVCOM are the WRF-FVCOM 10-member ensemble mean.

More specifically, WRF-FVCOM captures the west-to-east movement of the storm by replicating the initial decrease and the subsequent increase of air temperature over Buoy 45005 in the western basin of Lake Erie. The drop in air temperature signifies the arrival of the storm's cold air mass from the west while the rise in air temperature signifies the passing of the storm's cold air mass to the east. WRF-FVCOM's accurate representation

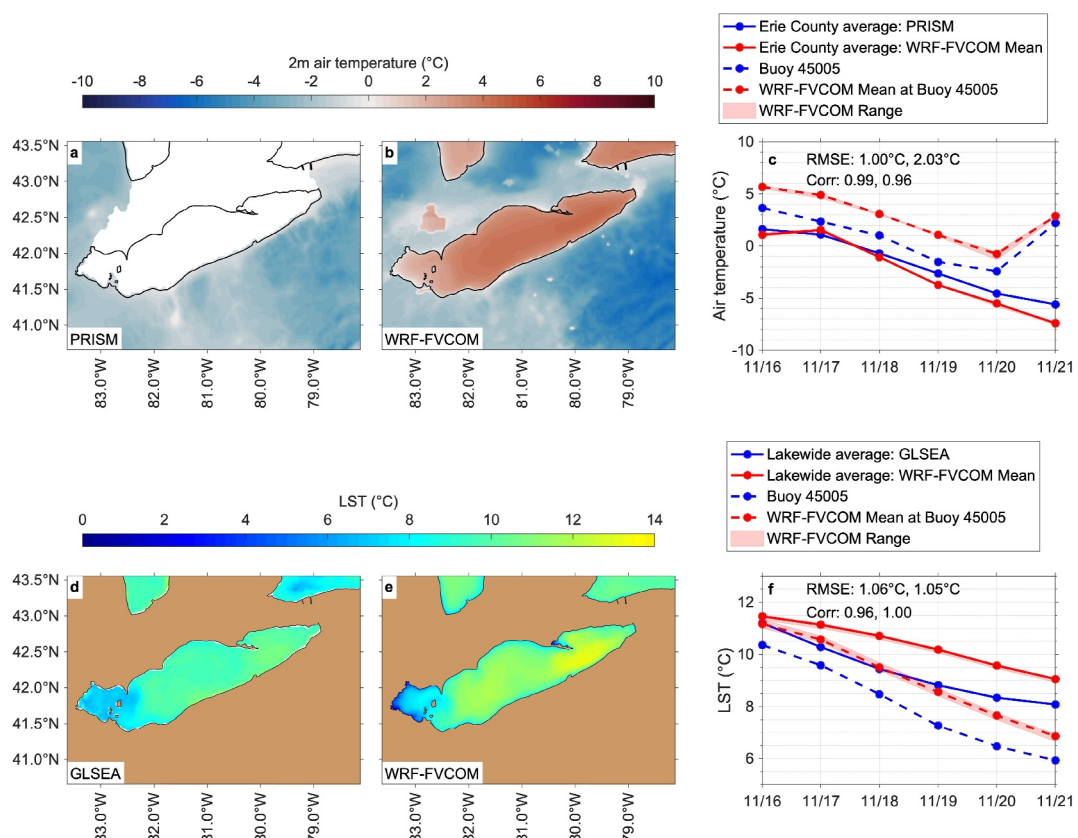


**Figure 6.** Model-observation comparison for air temperature and LST. Spatial comparison of air temperature (a, b) and temporal comparison of air temperature (c). Spatial comparison of LST (d, e) and temporal comparison of LST (f). The spatial maps show the average air temperature and LST during November 16–21, 2022. The values for WRF-FVCOM in b and e are the WRF-FVCOM 10-member ensemble mean. The red shading in c and f is the range of the WRF-FVCOM ensemble. The RMSE and correlation for air temperature in c are provided for WRF-FVCOM against PRISM and Buoy 45005, in that order. The RMSE and correlation for LST in f are provided for WRF-FVCOM against GLSEA and Buoy 45005, in that order.

of the storm's west-to-east movement is also evident in the air temperature evolution over Erie County, which is situated to the east of Lake Erie. WRF-FVCOM accurately depicts the initial muted change and the subsequent swift decrease in air temperature over Erie County, implying the arrival of the storm's cold air mass.

The spatial LST heterogeneity seen in GLSEA for Lake Erie with warmer waters in the eastern basin and much cooler waters in the shallow western basin is also well reproduced by WRF-FVCOM (Figures 6d and 6e). The decreasing trend in the LST during the storm due to an increase in outgoing latent heat is also well captured by WRF-FVCOM (Figure 6f). Notably, the slower decline in lakewide average LST, in contrast to the rapid decline in LST at Buoy 45005, illustrates WRF-FVCOM's ability to represent the spatial variation in LST trend due to the west-to-east movement of the storm.

### 3.2. Buffalo LES Storm Under a Warmer Future Climate

The impact of a warmer future climate on the Buffalo LES storm precipitation (rainfall and snowfall) over Erie County is summarized in Figure 7. Specifically, we examined how the storm could evolve under the warmer mid-century and end-century climates (Figure 7a). We also assessed the storm's evolution under distinct isolated warming scenarios, namely under the isolated warming of the atmosphere to the mid-century and end-century levels (Figure 7b) and under the isolated warming of the lake to the mid-century and end-century levels (Figure 7c).

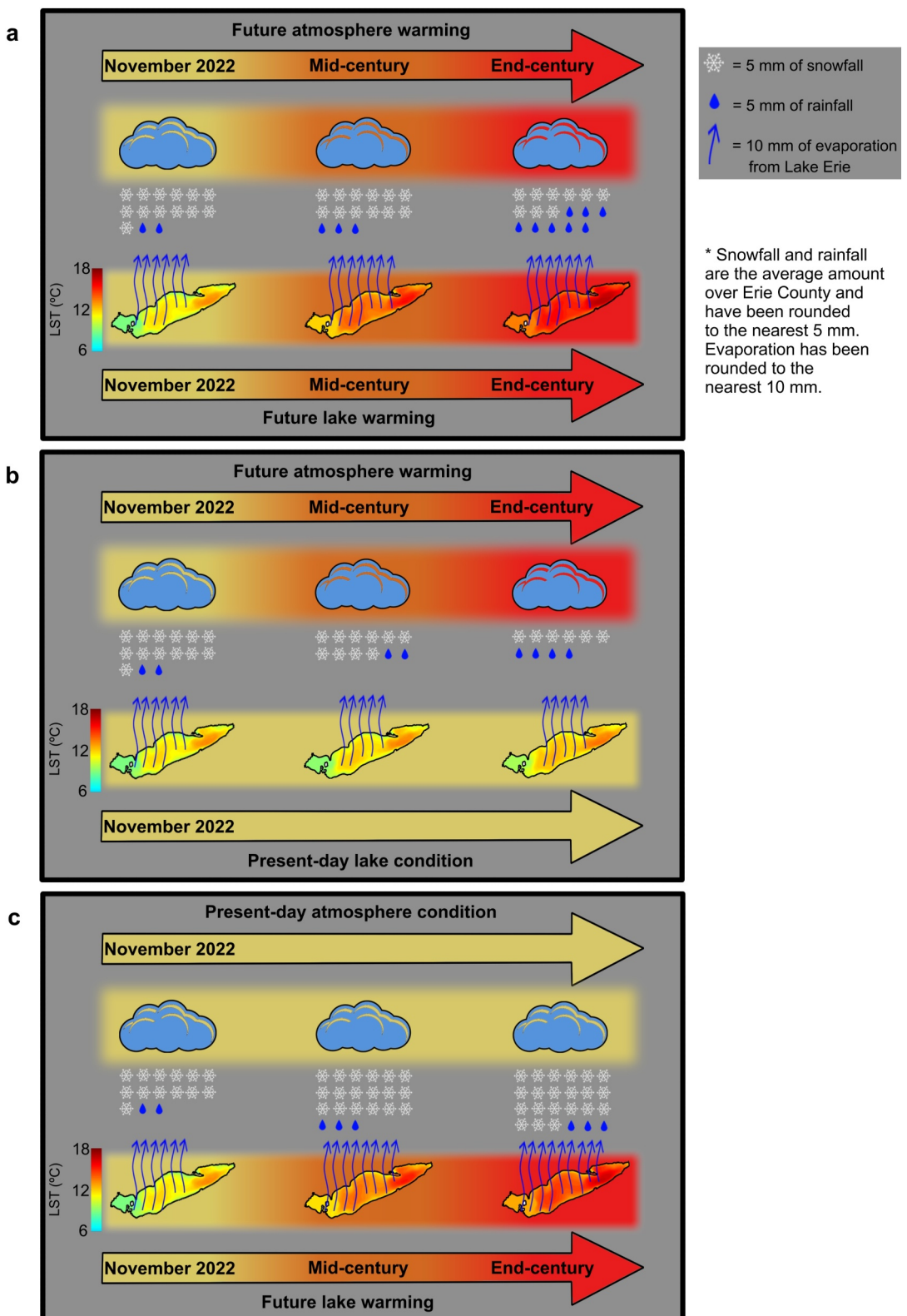


**Figure 7.** Impact of various future warming scenarios on the Buffalo LES storm precipitation. Changes in the storm when the climate (i.e., both the atmosphere and lake) are warmed to future levels (a). Changes in the storm when only the atmosphere is warmed to future levels (b). Changes in the storm when only the lake is warmed to future levels (c). The rainfall and snowfall are the total amount over Erie County for November 16–21. The evaporation is the total evaporation from Lake Erie during November 16–21. The LST is the average LST during November 16–21. The values are the WRF-FVCOM's 10-member ensemble mean.

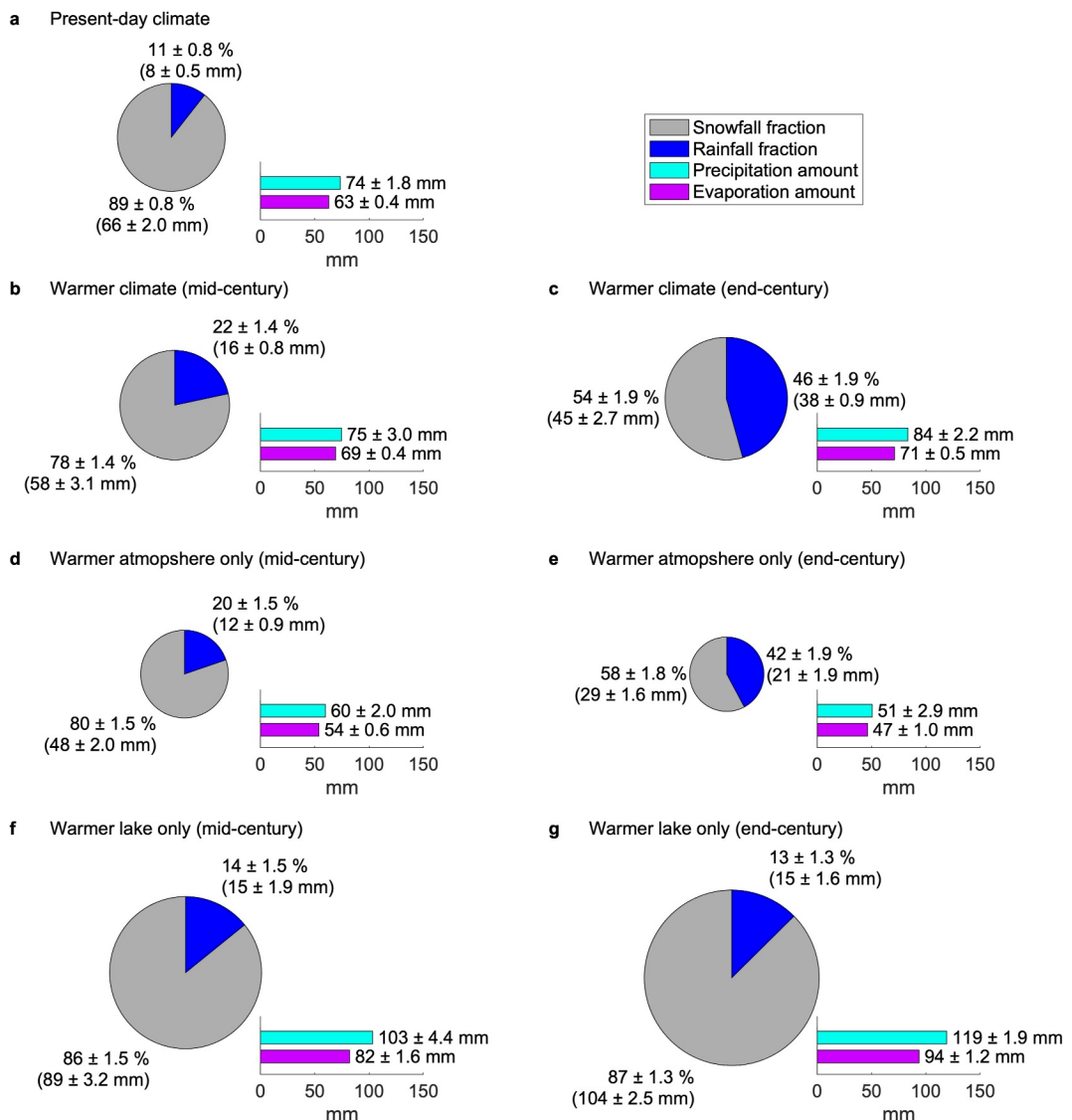


**Figure 8.** Snowfall fraction, rainfall fraction, precipitation, and lake evaporation under various future warming scenarios. Snowfall fraction, rainfall fraction, total precipitation over Erie County, and total lake evaporation during November 16–21 under various future warming scenarios. The snowfall and rainfall totals over Erie County are provided in parentheses. The size of the pie charts is proportional to the total storm precipitation over Erie County. The values are the WRF-FVCOM's 10-member ensemble mean and standard deviation.

The evolutions of LST and lake evaporation are also presented in Figure 7 as the primary source of moisture for LES storms is evaporation. To complement Figures 7 and 8 explicitly provides rainfall fraction and snowfall fraction as well as the magnitude of storm precipitation, rainfall, snowfall, and evaporation under the various future warming scenarios. The changes in the spatial and temporal patterns of key storm variables under the warming scenarios are provided in Figures S2–S5 in Supporting Information S1.

When compared to the present-day climate, the total LES storm precipitation is enhanced under the warmer mid-century and end-century climates (Figures 7a, 8b and 8c). The total storm precipitation over Erie County during the storm increases by around 1.3% (1 mm) in the moderately warmer climate of mid-century and more significantly by 13.5% (10 mm) in the considerably warmer climate of end-century, showing an accelerated rise in LES storm precipitation in the future. Moreover, there are significant changes in the snowfall and rainfall fraction in the future. Snowfall accounted for most (89%) of the total storm precipitation in the present-day climate, while in the warmer climates of mid-century and end-century, snowfall makes up only around three-quarters (78%) and

half (54%) of the total storm precipitation, respectively. Consequently, the proportion of rainfall increased from around one-tenth (11%) of the total storm precipitation in the present-day climate to around one-fifth (22%) and half (46%) of the total storm precipitation under the mid-century and end-century climates, respectively. Such increases in the storm's precipitation and rainfall fraction are consistent with the long-term projections from previous studies such as Notaro, Bennington, and Vavrus (2015) that projected increases in mean LES precipitation with an increase in rainfall at the expense of snowfall over the Great Lakes basin.

The mid-century and end-century changes in the storm precipitation are intricately linked to the dynamic interplay between the warmer atmosphere and warmer lake. However, the precise influence of a warmer atmosphere and a warmer lake – particularly their role in shaping the future storm precipitation characteristics is uncertain. It is unclear whether a warmer atmosphere and a warmer lake yield complementary or conflicting changes to the storm precipitation because previous models were unable to accurately describe the lake processes and their interactions with the atmosphere. To that end, we isolated the distinct impacts of a warmer atmosphere (Figures 7b, 8d and 8e) and a warmer lake (Figures 7c, 8f and 8g) on the storm, focusing on a mechanistic understanding of the changes in storm precipitation under warmer future climates.

Compared to the present-day climate, the isolated warming of the atmosphere resulted in a higher rainfall fraction at the expense of snowfall. The rainfall fraction increased from 11% under the present-day climate to 20% and 42% under the isolated warmer atmosphere of mid-century and end-century, respectively. These rainfall fractions under the warmer atmosphere are close to those produced under the warmer mid-century and end-century climates, where both the lake and atmosphere are at their warmer future conditions. Hence, the higher rainfall fraction under the warmer future climates, relative to the present-day climate, is primarily attributable to the warmer future atmosphere. In other words, future warming of the atmosphere is the main factor that determines the partitioning LES storm precipitation into rainfall and snowfall.

However, in contrast to the warmer future climates with warmer atmosphere and lake, which yielded a higher amount of total storm precipitation relative to the present-day climate, an isolated warming of the atmosphere produced lower storm precipitation relative to the present-day climate. The total storm precipitation over Erie County decreased from 74 mm under the present-day climate to 60 and 51 mm under the isolated warmer atmosphere of mid-century and end-century, respectively. This decrease in the total storm precipitation is a result of Lake Erie's diminished evaporation, which is due to the fact that an isolated warming of the atmosphere results in a lower specific humidity gradient at the lake-atmosphere interface during cold seasons. The evaporation decreased from 63 mm under the present-day climate to 54 and 47 mm under the isolated warmer atmosphere of mid-century and end-century, respectively. Therefore, the warmer future atmosphere is not primarily responsible for the higher storm precipitation under the warmer future climates.

Instead, the higher storm precipitation under the warmer future climates relative to the present-day climate is explained by the warmer future lake feeding the atmosphere with more moisture through evaporation for the LES storm. The elevated LST during the cold season induces a higher specific humidity gradient over the lake surface, thereby intensifying evaporation and consequently leading to an increase in moisture supply that supports a higher amount of storm precipitation. This underlying mechanism behind the increase in storm precipitation through increased evaporation is demonstrated in Figures 7c, 8f and 8g, which summarizes the evolution of the Buffalo LES storm under an isolated warming of the lake. Future warming is not applied to the atmosphere in this scenario; thus, the atmosphere still mostly reflects the present-day climate. The isolated warming of the lake, therefore, results in a particularly large specific humidity gradient over the lake and provides a clear representation of the link between the increase in evaporation and the increase in storm precipitation. Specifically, Lake Erie's evaporation increased from 63 mm under the present-day climate to 82 and 94 mm under the isolated warmer lake of mid-century and end-century, respectively. As a result, the total storm precipitation increased from 74 mm under the present-day climate to 103 and 119 mm under the isolated warmer lake of mid-century and end-century, respectively.

It is also important to note that, under the isolated warming of the lake, snowfall continues to be the predominant form of precipitation, with a very similar snowfall fraction to that of the present-day climate. Snowfall accounts for 89% of the total storm precipitation under the present-day climate, and it remains high at 86% and 87% of total precipitation under the isolated warmer lake of mid-century and end-century, respectively. This reinforces that, in a warmer future climate, the primary determinant of storm precipitation type, whether it is rainfall or snowfall, is the atmosphere temperature. On the other hand, the amount of storm precipitation under a warmer future climate

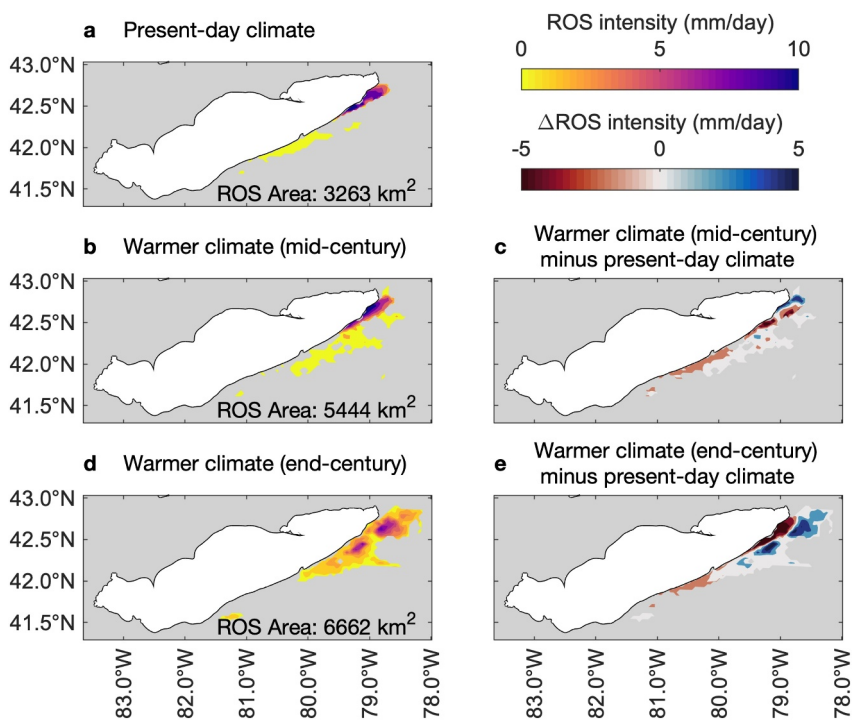


**Figure 9.** Rain-on-snow (ROS) intensity under warmer future climates. Mean ROS intensity and the total area experiencing ROS during November 16–20 (a, b, d). Difference in mean ROS intensity between warmer future climate and the present-day climate (c, e). The values are the WRF-FVCOM's 10-member ensemble mean.

is determined by the relative warming of the atmosphere and lake. Their relative warming shapes the moisture gradient at the lake-atmosphere interface, thereby leading to changes in lake evaporation and consequently precipitation. The rise in the Buffalo LES storm's precipitation amount under the mid-century and end-century climates, relative to the present-day climate, is, therefore, an outcome of the relative warming of the atmosphere and lake, with increased evaporation from a warmer Lake Erie contributing to the higher storm precipitation.

### 3.3. Impact of Changes in the Buffalo LES Storm on Concurrent ROS

Under a warmer future climate, the shift of storm precipitation from snowfall to rainfall could amplify other winter hazards such as ROS (Freudiger et al., 2014; Li et al., 2019; McCabe et al., 2007; Musselman et al., 2018). In our study, the increase in storm rainfall under the warmer future climates notably increases the total area experiencing ROS during the LES storm (Figure 9). The total area experiencing ROS in the vicinity of Lake Erie is more than doubled under the warmer future climate of the end-century when compared to the area under the present-day climate. Areas that did not experience ROS under the present-day climate exhibit ROS intensities (sum of snowmelt and rainfall) of up to 5 mm/day under the warmer future climate. On the other hand, some areas experience a decrease in ROS intensity under a warmer future climate due to a decrease in the snowpack. This suggests that the warmer future climate could both mitigate and exacerbate ROS through changes in the LES storm. Therefore, the changes in one winter hazard due to changes in another amid climate change, along with the compounding impact of concurrent winter hazards on the vulnerable communities, warrants a more forensic investigation in future studies.

## 4. Discussion and Conclusion

In this study, by employing WRF-FVCOM and warming the lake and the overlying atmosphere during the storm to the projected future condition using the PGW method, we created a storyline that describes a physically self-consistent unfolding of the Buffalo LES storm under the warmer future climate. WRF-FVCOM revealed an increase in the total storm precipitation amount by up to 14% under the warmer future climate, accompanied by a

shift in the storm precipitation form from predominantly snowfall to nearly equal parts snowfall and rainfall. Through additional WRF-FVCOM simulations with isolated atmospheric and lake warming, we discerned that the higher storm rainfall fraction is a consequence of a warmer atmosphere while the higher storm precipitation is primarily a consequence of the intensified evaporation from a warmer lake.

The critical role of evaporation in the amount of storm precipitation is further reinforced by its high relative contribution to the storm precipitation amount among the various moisture budget components (Figure S6 in Supporting Information S1). Evaporation from Lake Erie alone accounts for 76% of the total moisture for storm precipitation under the present-day climate and the warmer future climate. Moreover, our findings on increased lake evaporation under warmer future climates also align with the evaporation projections from previous hydroclimate research that used long-term dynamical downscaling of GCMs (Kayastha et al., 2022; Mailhot et al., 2019; Notaro, Bennington, & Lofgren, 2015; Notaro, Bennington, & Vavrus, 2015). As such, the continued dominance of evaporation as a moisture source and a consensus among studies for the projected increase emphasize evaporation's importance in understanding future LES storms in the region.

Additionally, when comparing the evaporation amount during the storm under the warmer future climate and under the isolated warming scenarios, the evaporation decreases by as much as 34% under the isolated warming of the atmosphere and increases by up to 32% under the isolated warming of the lake. Such variation in the evaporation amount emphasizes the significance of accurately resolving both the atmosphere and lake warming when studying the future evolution of LES storms, as failure to do so might lead to significant underestimation or overestimation of evaporation and ultimately result in a misrepresentation of LES storm precipitation amount. In other words, an accurate representation of the Great Lakes through a comprehensive two-way coupled 3D lake model within a regional climate modeling system is paramount for studying the future evolution of LES storms because a dynamically accurate representation of the Great Lakes is essential in achieving an accurate degree of future lake warming and evaporation.

Furthermore, under a warmer future climate, the projected decrease in the Great Lakes ice cover toward a nearly ice-free system could significantly enhance winter evaporation during the months (e.g., January–March) that, under the present-day climate, typically experience high ice cover with restricted evaporation and limited LES storms (Notaro, Bennington, & Vavrus, 2015; Shi & Xue, 2019; Xue et al., 2022). Consequently, a warmer future climate could drastically extend the LES storm season into the current ice cover season by removing ice cover, which creates more favorable conditions for evaporation and subsequent LES storms (Vavrus et al., 2013). In this study's context, the Great Lakes were virtually ice-free during the Buffalo LES storm, and the impact of declining ice cover in the future could not be examined. Therefore, there is a need for future studies to focus on the interseasonal changes in the Great Lakes resulting from climate change and their subsequent influence on LES storms. This can be achieved by systematically examining the occurrence, duration, and severity of LES through a large number of simulations across different atmospheric, lake, and ice scenarios under various winter conditions.

Lastly, the PGW method used in the storyline framework does not consider potential future changes in the interannual variability of synoptic systems since the historical synoptic environment is inherited by the PGW simulations (Brogli et al., 2023). Nevertheless, storylines through PGW have been widely used to understand and derive plausible future scenarios of extreme historical events because of its multiple advantages including the improvement of risk awareness by framing risk in an event-oriented perspective, which aligns more closely with how people perceive and respond to risk. Our storyline provides one of many plausible futures for the Buffalo LES storm and answers the societally relevant question of what could happen to the storm under a warmer climate (Shepherd, 2019). The storyline approach, therefore, weaves together a coherent story that outlines how various climate processes and interactions might lead to certain changes in LES storms. It provides a mechanistic understanding of the driving factors involved and their influences on the future evolution of LES storms by exploring the manifestation of the Buffalo LES storm through distinct warming of the atmosphere and lake. Our storyline in this study also explored the boundaries of plausible futures of LES storms by studying a record-breaking storm under the high-end emission scenario of SSP5-8.5. Hence, our study operates within the scope of the storyline and PGW strategies. While the approach does not represent the climate change-induced variability in the entire spectrum of LES storms that is, storms developing from different synoptic systems, our study provides a valuable framework and analysis for understanding LES storms in the Great Lakes region. Our study underscored the importance for a fully 3D two-way lake-atmosphere coupling to accurately simulate the LES storms under the present-day and future climates. Failure to capture the lake-atmosphere interaction and

coevolution, such as in a storyline only resolving the atmospheric warming, would result in significant misrepresentation of future LES storms.

## Data Availability Statement

The source codes for the two-way coupled FVCOM and WRF used in this study are available at <https://doi.org/10.5281/zenodo.7574673> (Huang, 2023a) and <https://doi.org/10.5281/zenodo.7574675> (Huang, 2023b) respectively. The National Centers for Environmental Information (NCEI) Storm Event Database can be accessed at <https://www.ncdc.noaa.gov/stormevents/> (NCEI, 2023). Observation data sets used in this study may be openly accessed and downloaded at the following webpages: ERA5: <https://doi.org/10.24381/cds.adbb2d47> (Hersbach et al., 2023), StageIV: <https://data.eol.ucar.edu/dataset/21.093> (Du, 2011), PRISM: <https://prism.oregonstate.edu/> (PRISM Climate Group, 2016), SNODAS: <https://nsidc.org/data/g02158 VERSIONS/1> (NOHRSC, 2004), UA: <https://nsidc.org/data/nsidc-0719 VERSIONS/1> (Broxton et al., 2019), NDBC: <https://www.ndbc.noaa.gov/> (NDBC, 2023) and GLSEA: <https://coastwatch.glerl.noaa.gov/glsea/doc/> (GLSEA, 2023).

## Acknowledgments

This study is supported by COMPASS-GLM, a multi-institutional project supported by the U.S. Department of Energy, Office of Science, Office of Biological and Environmental Research as part of the Regional and Global Modeling and Analysis (RGMA) program, Multi-sector Dynamics Modeling (MSD) program, and Earth System Model Development (ESMD) program. Computational resources are provided by the DOE-supported National Energy Research Scientific Computing Center and Argonne Leadership Computing Facility. Computational resources are also provided by Michigan Tech through their high-performance computing cluster, Superior. This is Contribution No. 118 of the Great Lakes Research Center at Michigan Tech.

## References

- Akinsanola, A. A., Jung, C., Wang, J., & Kotamarthi, V. R. (2024). Evaluation of precipitation across the contiguous United States, Alaska, and Puerto Rico in multi-decadal convection-permitting simulations. *Scientific Reports*, 14(1), 1238.
- Alcott, T. I., & Steenburgh, W. J. (2013). Orographic influences on a Great Salt Lake–effect snowstorm. *Monthly Weather Review*, 141(7), 2432–2450.
- Anderson, E. J., Fujisaki-Manome, A., Kessler, J., Lang, G. A., Chu, P. Y., Kelley, J. G. W., et al. (2018). Ice forecasting in the next-generation Great Lakes operational forecast system (GLOFS). *Journal of Marine Science and Engineering*, 6(4), 123. Retrieved from <https://www.mdpi.com/2077-1312/6/4/123>
- Ayon, B. D., Ofori-Amoah, B., Meng, L., Oh, J.-S., & Baker, K. (2020). Modeling the effects of lake-effect snow related weather conditions on daily traffic crashes: A time series count data approach. *Accident Analysis & Prevention*, 144, 105510. <https://doi.org/10.1016/j.aap.2020.105510>
- Bajjnath-Rodino, J. A., & Duguay, C. R. (2019). Assessment of coupled CRCM5–FLake on the reproduction of wintertime lake-induced precipitation in the Great Lakes Basin. *Theoretical and Applied Climatology*, 138(1), 77–96. <https://doi.org/10.1007/s00704-019-02799-8>
- Benjamin, S. G., Weygandt, S. S., Brown, J. M., Hu, M., Alexander, C. R., Smirnova, T. G., et al. (2016). A North American hourly assimilation and model forecast cycle: The rapid refresh. *Monthly Weather Review*, 144(4), 1669–1694. <https://doi.org/10.1175/MWR-D-15-0242.1>
- Bennington, V., Notaro, M., & Holman, K. D. (2014). Improving climate sensitivity of deep lakes within a regional climate model and its impact on simulated climate. *Journal of Climate*, 27(8), 2886–2911. <https://doi.org/10.1175/jcli-d-13-00110.1>
- Briley, L. J., Rood, R. B., & Notaro, M. (2021). Large lakes in climate models: A Great Lakes case study on the usability of CMIP5. *Journal of Great Lakes Research*, 47(2), 405–418. <https://doi.org/10.1016/j.jglr.2021.01.010>
- Brogli, R., Heim, C., Mensch, J., Sørland, S. L., & Schär, C. (2023). The pseudo-global-warming (PGW) approach: Methodology, software package PGW4ERA5 v1.1, validation, and sensitivity analyses. *Geoscientific Model Development*, 16(3), 907–926.
- Broxton, P., Zeng, X., & Dawson, N. (2019). Daily 4 km gridded SWE and snow depth from assimilated in-situ and modeled data over the conterminous US, version 1 [Dataset]. NASA National Snow and Ice Data Center Distributed Active Archive Center. <https://doi.org/10.5067/0GGPB220EX6A>
- Burnett, A. W., Kirby, M. E., Mullins, H. T., & Patterson, W. P. (2003). Increasing Great Lake–effect snowfall during the twentieth century: A regional response to global warming? *Journal of Climate*, 16(21), 3535–3542.
- Chen, C., Beardsley, R., & Cowles, G. (2006). An unstructured-grid finite-volume coastal Ocean Model (FVCOM) system. *Oceanography*, 19, 78–89. <https://doi.org/10.5670/oceanog.2006.92>
- Chen, C., Beardsley, R., Cowles, G., Qi, J., Lai, Z., Gao, G., et al. (2013). An unstructured-grid, finite-volume Community Ocean Model: FVCOM user manual (4th edn). SMAST/UMASSD Technical Report-13-0701.
- Corcoran, M. C., Thomas, E. K., & Boutt, D. F. (2019). Event-based precipitation isotopes in the Laurentian Great Lakes region reveal spatiotemporal patterns in moisture recycling. *Journal of Geophysical Research: Atmospheres*, 124(10), 5463–5478. <https://doi.org/10.1029/2018JD029545>
- Craig, A., Valcke, S., & Coquart, L. (2017). Development and performance of a new version of the OASIS coupler, OASIS3-MCT\_3.0. *Geoscientific Model Development*, 10(9), 3297–3308. <https://doi.org/10.5194/gmd-10-3297-2017>
- Daly, C., Halbleib, M., Smith, J. I., Gibson, W. P., Doggett, M. K., Taylor, G. H., et al. (2008). Physiographically sensitive mapping of climatological temperature and precipitation across the conterminous United States. *International Journal of Climatology: a Journal of the Royal Meteorological Society*, 28(15), 2031–2064.
- Daly, C., Neilson, R. P., & Phillips, D. L. (1994). A statistical-topographic model for mapping climatological precipitation over mountainous terrain. *Journal of Applied Meteorology and Climatology*, 33(2), 140–158.
- Dewey, K. F. (1977). Lake-Effect snowstorms and the record breaking 1976–77 snowfall to the lee of Lakes Erie and Ontario. *Weatherwise*, 30(6), 228–232. <https://doi.org/10.1080/00431672.1977.9931836>
- Dominguez, F., Dall'erba, S., Huang, S., Avelino, A., Mehran, A., Hu, H., et al. (2018). Tracking an atmospheric river in a warmer climate: From water vapor to economic impacts. *Earth System Dynamics*, 9(1), 249–266. <https://doi.org/10.5194/esd-9-249-2018>
- Du, J. (2011). NCEP/EMC 4KM gridded data (GRIB) stage IV data. Version 1.0 [Dataset]. UCAR/NCAR - Earth Observing Laboratory. <https://doi.org/10.5065/D6PG1QDD>
- Eckstein, D., Küntzel, V., & Schäfer, L. (2021). The global climate risk index 2021: Bonn: Germanwatch.
- Freudiger, D., Kohn, I., Stahl, K., & Weiler, M. (2014). Large-scale analysis of changing frequencies of rain-on-snow events with flood-generation potential. *Hydrology and Earth System Sciences*, 18(7), 2695–2709. <https://doi.org/10.5194/hess-18-2695-2014>
- Fujisaki-Manome, A., Fitzpatrick, L. E., Gronewold, A. D., Anderson, E. J., Lofgren, B. M., Spence, C., et al. (2017). Turbulent heat fluxes during an extreme lake-effect snow event. *Journal of Hydrometeorology*, 18(12), 3145–3163. <https://doi.org/10.1175/jhm-d-17-0062.1>

- Fujisaki-Manome, A., Mann, G. E., Anderson, E. J., Chu, P. Y., Fitzpatrick, L. E., Benjamin, S. G., et al. (2020). Improvements to lake-effect snow forecasts using a one-way air–lake model coupling approach. *Journal of Hydrometeorology*, 21(12), 2813–2828. <https://doi.org/10.1175/JHM-D-20-0079.1>
- Fujisaki-Manome, A., Wright, D. M., Mann, G. E., Anderson, E. J., Chu, P., Jablonowski, C., & Benjamin, S. G. (2022). Forecasting lake-/sea-effect snowstorms, advancement, and challenges. *WIREs Water*, 9(4), e1594. <https://doi.org/10.1002/wat2.1594>
- Giorgi, F., Coppola, E., Solmon, F., Mariotti, L., Sylla, M. B., Bi, X., et al. (2012). RegCM4: Model description and preliminary tests over multiple CORDEX domains. *Climate Research*, 52, 7–29. Retrieved from <https://www.int-res.com/abstracts/cr/v52/p7-29/>
- Gutmann, E. D., Rasmussen, R. M., Liu, C., Ikeda, K., Bruyere, C. L., Done, J. M., et al. (2018). Changes in hurricanes from a 13-yr convection-permitting pseudo-global warming simulation. *Journal of Climate*, 31(9), 3643–3657. <https://doi.org/10.1175/JCLI-D-17-0391.1>
- Haberlie, A. M., & Ashley, W. S. (2019). Climatological representation of mesoscale convective systems in a dynamically downscaled climate simulation. *International Journal of Climatology*, 39(2), 1144–1153.
- Hazeleger, W., van den Hurk, B. J. J. M., Min, E., van Oldenborgh, G. J., Petersen, A. C., Stainforth, D. A., et al. (2015). Tales of future weather. *Nature Climate Change*, 5(2), 107–113. <https://doi.org/10.1038/nclimate2450>
- Hersbach, H., Bell, B., Berrisford, P., Biavati, G., Horányi, A., Muñoz Sabater, J., et al. (2023). ERA5 hourly data on single levels from 1940 to present. [Dataset]. *Copernicus Climate Change Service (C3S) Climate Data Store (CDS)*. <https://doi.org/10.24381/cds.adbb2d47>
- Hersbach, H., Bell, B., Berrisford, P., Hirahara, S., Horányi, A., Muñoz-Sabater, J., et al. (2020). The ERA5 global reanalysis. *Quarterly Journal of the Royal Meteorological Society*, 146(730), 1999–2049. <https://doi.org/10.1002/qj.3803>
- HolroydIII, E. W. (1971). Lake-effect cloud bands as seen from weather satellites. *Journal of the Atmospheric Sciences*, 28(7), 1165–1170.
- Huang, C. (2023a). FVCOM\_v41\_coupled\_code. [Software]. Zenodo. <https://doi.org/10.5281/zenodo.7574673>
- Huang, C. (2023b). WRFv422 coupled code. [Software]. Zenodo. <https://doi.org/10.5281/zenodo.7574675>
- Iacono, M. J., Delamere, J. S., Mlawer, E. J., Shephard, M. W., Clough, S. A., & Collins, W. D. (2008). Radiative forcing by long-lived greenhouse gases: Calculations with the AER radiative transfer models. *Journal of Geophysical Research*, 113(D13). <https://doi.org/10.1029/2008JD009944>
- Janjić, Z. I. (1994). The step-mountain eta coordinate model: Further developments of the convection, viscous sublayer, and turbulence closure schemes. *Monthly Weather Review*, 122(5), 927–945.
- Jung, C., & Lackmann, G. M. (2019). Extratropical transition of Hurricane Irene (2011) in a changing climate. *Journal of Climate*, 32(15), 4847–4871.
- Kayastha, M. B., Huang, C., Wang, J., Pringle, W. J., Chakraborty, T., Yang, Z., et al. (2023). Insights on simulating summer warming of the Great Lakes: Understanding the behavior of a newly developed coupled lake-atmosphere modeling system. *Journal of Advances in Modeling Earth Systems*, 15(7), e2023MS003620. <https://doi.org/10.1029/2023MS003620>
- Kayastha, M. B., Ye, X., Huang, C., & Xue, P. (2022). Future rise of the Great Lakes water levels under climate change. *Journal of Hydrology*, 612, 128205. <https://doi.org/10.1016/j.jhydrol.2022.128205>
- Kouadio, K., Bastin, S., Konare, A., & Ajayi, V. O. (2020). Does convection-permitting simulate better rainfall distribution and extreme over Guinean coast and surroundings? *Climate Dynamics*, 55(1), 153–174.
- Kunkel, K. E., Westcott, N. E., & Kristovich, D. A. (2002). Assessment of potential effects of climate change on heavy lake-effect snowstorms near Lake Erie. *Journal of Great Lakes Research*, 28(4), 521–536.
- Li, D., Lettenmaier, D. P., Margulis, S. A., & Andreidis, K. (2019). The role of rain-on-snow in flooding over the conterminous United States. *Water Resources Research*, 55(11), 8492–8513. <https://doi.org/10.1029/2019WR024950>
- Mailhot, E., Music, B., Nadeau, D. F., Frigon, A., & Turcotte, R. (2019). Assessment of the Laurentian Great Lakes' hydrological conditions in a changing climate. *Climatic Change*, 157(2), 243–259. <https://doi.org/10.1007/s10584-019-02530-6>
- McCabe, G. J., Clark, M. P., & Hay, L. E. (2007). Rain-on-snow events in the western United States. *Bulletin of the American Meteorological Society*, 88(3), 319–328. <https://doi.org/10.1175/BAMS-88-3-319>
- Meinshausen, M., Nicholls, Z. R. J., Lewis, J., Gidden, M. J., Vogel, E., Freund, M., et al. (2020). The shared socio-economic pathway (SSP) greenhouse gas concentrations and their extensions to 2500. *Geoscientific Model Development*, 13(8), 3571–3605. <https://doi.org/10.5194/gmd-13-3571-2020>
- Mellor, G. L., & Yamada, T. (1982). Development of a turbulence closure model for geophysical fluid problems. *Reviews of Geophysics*, 20(4), 851–875. <https://doi.org/10.1029/RG020i004p00851>
- Monin, A. S., & Obukhov, A. M. (1954). Basic laws of turbulent mixing in the surface layer of the atmosphere. *Contrib. Geophys. Inst. Acad. Sci. USSR*, 151(163), e187.
- Morrison, H., Curry, J., & Khvorostyanov, V. (2005). A new double-moment microphysics parameterization for application in cloud and climate models. Part I: Description. *Journal of the Atmospheric Sciences*, 62(6), 1665–1677.
- Musselman, K. N., Lehner, F., Ikeda, K., Clark, M. P., Prein, A. F., Liu, C., et al. (2018). Projected increases and shifts in rain-on-snow flood risk over western North America. *Nature Climate Change*, 8(9), 808–812. <https://doi.org/10.1038/s41558-018-0236-4>
- National Operational Hydrologic Remote Sensing Center (NOHRSC). (2004). Snow data assimilation system (SNODAS) data products at NSIDC, version 1 [Dataset]. *National Snow and Ice Data Center*. <https://doi.org/10.7265/N5TB14TC>
- Niu, G.-Y., Yang, Z.-L., Mitchell, K. E., Chen, F., Ek, M. B., Barlage, M., et al. (2011). The community Noah land surface model with multiparameterization options (Noah-MP): 1. Model description and evaluation with local-scale measurements. *Journal of Geophysical Research*, 116(D12). <https://doi.org/10.1029/2010JD015139>
- NOAA Great Lakes Surface Environmental Analysis (GLSEA). (2023). Sea surface temperature (SST) from Great lakes surface environmental analysis (GLSEA). [Dataset]. *National Oceanic and Atmospheric Administration*. Retrieved from [https://coastwatch.glerl.noaa.gov/erddap/files/GLSEA\\_GCS/](https://coastwatch.glerl.noaa.gov/erddap/files/GLSEA_GCS/)
- NOAA National Centers for Environmental Information (NCEI). (2023). Storm event Database. [Dataset]. *National Oceanic and Atmospheric Administration*. Retrieved from <https://www.ncdc.noaa.gov/stormevents/>
- NOAA National Data Buoy Center (NDBC). (2023). National data buoy center. [Dataset]. *National Oceanic and Atmospheric Administration*. Retrieved from <https://www.ndbc.noaa.gov/>
- NOAA National Weather Service (NWS). (2006). Lake effect snow event archive: October 12, 2006 to october 13, 2006. Retrieved from [https://www.weather.gov/buf/lesEventArchive2006-2007\\_a](https://www.weather.gov/buf/lesEventArchive2006-2007_a)
- NOAA National Weather Service (NWS). (2014a). Lake effect summary: November 17-19, 2014. Retrieved from [https://www.weather.gov/buf/lake1415\\_stormb.html](https://www.weather.gov/buf/lake1415_stormb.html)
- NOAA National Weather Service (NWS). (2014b). Lake effect summary: November 19-21, 2014. Retrieved from [https://www.weather.gov/buf/lake1415\\_stormc.html](https://www.weather.gov/buf/lake1415_stormc.html)

- NOAA National Weather Service (NWS). (2022). Lake effect snow event archive. Retrieved from <https://www.weather.gov/buf/lesEventArchive?season=2022-2023&event=A>
- Notaro, M., Bennington, V., & Lofgren, B. (2015). Dynamical downscaling-based projections of Great Lakes water Levels\*. *Journal of Climate*, 28(24), 9721–9745. <https://doi.org/10.1175/jcli-d-14-00847.1>
- Notaro, M., Bennington, V., & Vavrus, S. (2015). Dynamically downscaled projections of Lake-effect snow in the Great Lakes basin\*. *Journal of Climate*, 28, 1661–1684. <https://doi.org/10.1175/JCLI-D-14-00467.1>
- Notaro, M., Zarrin, A., Vavrus, S., & Bennington, V. (2013). Simulation of heavy Lake-effect snowstorms across the Great Lakes basin by RegCM4: Synoptic climatology and Variability\*,+. *Monthly Weather Review*, 141(6), 1990–2014. <https://doi.org/10.1175/mwr-d-11-00369.1>
- Patricola, C. M., & Wehner, M. F. (2018). Anthropogenic influences on major tropical cyclone events. *Nature*, 563(7731), 339–346.
- Prein, A. F., Rasmussen, R. M., Ikeda, K., Liu, C., Clark, M. P., & Holland, G. J. (2017). The future intensification of hourly precipitation extremes. *Nature Climate Change*, 7(1), 48–52.
- PRISM Climate Group. (2016). PRISM climate data. [Dataset]. *PRISMA climate group*. Retrieved from <https://prism.oregonstate.edu/>
- Qing, Y., & Wang, S. (2021). Multi-decadal convection-permitting climate projections for China's Greater Bay Area and surroundings. *Climate Dynamics*, 57(1), 415–434. <https://doi.org/10.1007/s00382-021-05716-w>
- Riahi, K., Rao, S., Krey, V., Cho, C., Chirkov, V., Fischer, G., et al. (2011). RCP 8.5—A scenario of comparatively high greenhouse gas emissions. *Climatic Change*, 109(1), 33. <https://doi.org/10.1007/s10584-011-0149-y>
- Schär, C., Frei, C., Lüthi, D., & Davies, H. C. (1996). Surrogate climate-change scenarios for regional climate models. *Geophysical Research Letters*, 23(6), 669–672. <https://doi.org/10.1029/96GL00265>
- Schmidlin, T. W., & Kosarik, J. (1999). A record Ohio snowfall during 9–14 November 1996. *Bulletin of the American Meteorological Society*, 80(6), 1107–1116.
- Schwab, D. J., Leshkevich, G. A., & Muhr, G. C. (1999). Automated mapping of surface water temperature in the Great lakes. *Journal of Great Lakes Research*, 25(3), 468–481. [https://doi.org/10.1016/S0380-1330\(99\)70755-0](https://doi.org/10.1016/S0380-1330(99)70755-0)
- Seneviratne, S. I., Zhang, X., Adnan, M., Badi, W., Dereczynski, C., Di Luca, A., et al. (2021). *Weather and climate extreme events in a changing climate*. Cambridge University Press.
- Shepherd, T. G. (2019). Storyline approach to the construction of regional climate change information. *Proceedings of the Royal Society A: Mathematical, Physical and Engineering Sciences*, 475(2225), 20190013. <https://doi.org/10.1098/rspa.2019.0013>
- Shepherd, T. G., Boyd, E., Calel, R. A., Chapman, S. C., Dessai, S., Dima-West, I. M., et al. (2018). Storylines: An alternative approach to representing uncertainty in physical aspects of climate change. *Climatic Change*, 151, 555–571.
- Shi, Q., & Xue, P. (2019). Impact of Lake surface temperature variations on lake effect snow over the Great Lakes region. *Journal of Geophysical Research: Atmospheres*, 124(23), 12553–12567. <https://doi.org/10.1029/2019jd031261>
- Skamarock, W. C., & Klemp, J. B. (2008). A time-split nonhydrostatic atmospheric model for weather research and forecasting applications. *Journal of Computational Physics*, 227(7), 3465–3485. <https://doi.org/10.1016/j.jcp.2007.01.037>
- Smagorinsky, J. (1963). General circulation experiments with the primitive equations: I. The basic experiment. *Monthly Weather Review*, 91(3), 99–164. [https://doi.org/10.1175/1520-0493\(1963\)091<0099:Gcewtp>2.3.Co;2](https://doi.org/10.1175/1520-0493(1963)091<0099:Gcewtp>2.3.Co;2)
- Sun, L., Liang, X.-Z., & Xia, M. (2020). Developing the coupled CWRF-FVCOM modeling system to understand and predict atmosphere-watershed interactions over the Great lakes region. *Journal of Advances in Modeling Earth Systems*, 12(12), e2020MS002319. <https://doi.org/10.1029/2020MS002319>
- Sun, X., Xue, M., Brotzge, J., McPherson, R. A., Hu, X. M., & Yang, X. Q. (2016). An evaluation of dynamical downscaling of Central Plains summer precipitation using a WRF-based regional climate model at a convection-permitting 4 km resolution. *Journal of Geophysical Research: Atmospheres*, 121(23), 13801–813825. <https://doi.org/10.1002/2016JD024796>
- Suriano, Z. J., & Leathers, D. J. (2016). Twenty-first century snowfall projections within the eastern Great lakes region: Detecting the presence of A lake-induced snowfall signal in GCMs. *International Journal of Climatology*, 36(5), 2200–2209.
- Suriano, Z. J., & Leathers, D. J. (2017). Synoptically classified lake-effect snowfall trends to the lee of Lakes Erie and Ontario. *Climate Research*, 74(1), 1–13.
- Ullrich, P. A., Xu, Z., Rhoades, A. M., Dettinger, M. D., Mount, J. F., Jones, A. D., & Vahmani, P. (2018). California's drought of the future: A midcentury recreation of the exceptional conditions of 2012–2017. *Earth's Future*, 6(11), 1568–1587. <https://doi.org/10.1029/2018EF001007>
- Umek, L., & Gohm, A. (2016). Lake and orographic effects on a snowstorm at Lake constance. *Monthly Weather Review*, 144(12), 4687–4707. <https://doi.org/10.1175/MWR-D-16-0032.1>
- Vavrus, S., Notaro, M., & Zarrin, A. (2013). The role of ice cover in heavy Lake-Effect snowstorms over the Great Lakes basin as simulated by RegCM4. *Monthly Weather Review*, 141(1), 148–165. <https://doi.org/10.1175/MWR-D-12-00107.1>
- Veals, P. G., & Steenburgh, W. J. (2015). Climatological characteristics and orographic enhancement of lake-effect precipitation east of Lake Ontario and over the Tug Hill Plateau. *Monthly Weather Review*, 143(9), 3591–3609.
- Wang, J., Xue, P., Pringle, W., Yang, Z., & Qian, Y. (2022). Impacts of Lake surface temperature on the summer climate over the Great lakes region. *Journal of Geophysical Research: Atmospheres*, 127(11), e2021JD036231. <https://doi.org/10.1029/2021JD036231>
- Welsh, D., Geerts, B., Jing, X., Bergmaier, P. T., Minder, J. R., Steenburgh, W. J., & Campbell, L. S. (2016). Understanding heavy lake-effect snowfall: The vertical structure of radar reflectivity in a deep snowband over and downwind of Lake Ontario. *Monthly Weather Review*, 144(11), 4221–4244.
- Wiggan, B. L. (1950). Great snows of the Great Lakes. *Weatherwise*, 3(6), 123–126.
- Wiley, J., & Mercer, A. (2020). An updated synoptic climatology of Lake Erie and Lake Ontario heavy lake-effect snow events. *Atmosphere*, 11(8), 872.
- Wiley, J., & Mercer, A. (2021). Synoptic climatology of lake-effect snow events off the western Great Lakes. *Climate*, 9(3), 43. Retrieved from <https://www.mdpi.com/2225-1154/9/3/43>
- Wright, D. M., Posselt, D. J., & Steiner, A. L. (2013). Sensitivity of lake-effect snowfall to lake ice cover and temperature in the Great Lakes region. *Monthly Weather Review*, 141(2), 670–689.
- Xue, P., Pal, J. S., Ye, X., Lenters, J. D., Huang, C., & Chu, P. Y. (2017). Improving the simulation of large lakes in regional climate modeling: Two-way lake-atmosphere coupling with a 3D hydrodynamic model of the Great lakes. *Journal of Climate*, 30(5), 1605–1627. <https://doi.org/10.1175/jcli-d-16-0225.1>
- Xue, P., Ye, X., Pal, J. S., Chu, P. Y., Kayastha, M. B., & Huang, C. (2022). Climate projections over the Great lakes region: Using two-way coupling of a regional climate model with a 3-D lake model. *Geoscientific Model Development*, 15(11), 4425–4446. <https://doi.org/10.5194/gmd-15-4425-2022>

Yang, Z., Qian, Y., Liu, Y., Berg, L. K., Hu, H., Dominguez, F., & Huang, M. (2019). Irrigation impact on water and energy cycle during dry years over the United States using convection-permitting WRF and a dynamical recycling model. *Journal of Geophysical Research: Atmospheres*, 124(21), 11220–11241. <https://doi.org/10.1029/2019JD030524>

## References From the Supporting Information

- Bi, D., Dix, M., Marsland, S., O'farrell, S., Sullivan, A., Bodman, R., et al. (2020). Configuration and spin-up of ACCESS-CM2, the new generation Australian community climate and earth system simulator coupled model. *Journal of Southern Hemisphere Earth Systems Science*, 70(1), 225–251.
- Boucher, O., Servonnat, J., Albright, A. L., Aumont, O., Balkanski, Y., Bastrikov, V., et al. (2020). Presentation and evaluation of the IPSL-CM6A-LR climate model. *Journal of Advances in Modeling Earth Systems*, 12(7), e2019MS002010. <https://doi.org/10.1029/2019MS002010>
- Cherchi, A., Fogli, P. G., Lovato, T., Peano, D., Iovino, D., Gualdi, S., et al. (2019). Global mean climate and main patterns of variability in the CMCC-CM2 coupled model. *Journal of Advances in Modeling Earth Systems*, 11(1), 185–209. <https://doi.org/10.1029/2018MS001369>
- Golaz, J. C., Caldwell, P. M., Van Roekel, L. P., Petersen, M. R., Tang, Q., Wolfe, J. D., et al. (2019). The DOE E3SM coupled model version 1: Overview and evaluation at standard resolution. *Journal of Advances in Modeling Earth Systems*, 11(7), 2089–2129. <https://doi.org/10.1029/2018MS001603>
- Held, I., Guo, H., Adcroft, A., Dunne, J., Horowitz, L., Krasting, J., et al. (2019). Structure and performance of GFDL's CM4. 0 climate model. *Journal of Advances in Modeling Earth Systems*, 11(11), 3691–3727. <https://doi.org/10.1029/2019MS001829>
- Jungclaus, J. H., Fischer, N., Haak, H., Lohmann, K., Marotzke, J., Matei, D., et al. (2013). Characteristics of the ocean simulations in the Max Planck Institute Ocean Model (MPIOM) the ocean component of the MPI-Earth system model. *Journal of Advances in Modeling Earth Systems*, 5(2), 422–446. <https://doi.org/10.1002/jame.20023>
- Marsh, D. R., Mills, M. J., Kinnison, D. E., Lamarque, J.-F., Calvo, N., & Polvani, L. M. (2013). Climate change from 1850 to 2005 simulated in CESM1 (WACCM). *Journal of Climate*, 26(19), 7372–7391.
- Seland, Ø., Bentsen, M., Olivé, D., Tonizzo, T., Gjermundsen, A., Graff, L. S., et al. (2020). Overview of the Norwegian Earth System Model (NorESM2) and key climate response of CMIP6 DECK, historical, and scenario simulations. *Geoscientific Model Development*, 13(12), 6165–6200.
- Swart, N. C., Cole, J. N., Kharin, V. V., Lazare, M., Scinocca, J. F., Gillett, N. P., et al. (2019). The Canadian earth system model version 5 (CanESM5. 0.3). *Geoscientific Model Development*, 12(11), 4823–4873.
- Tatebe, H., Ogura, T., Nitta, T., Komuro, Y., Oogochi, K., Takemura, T., et al. (2019). Description and basic evaluation of simulated mean state, internal variability, and climate sensitivity in MIROC6. *Geoscientific Model Development*, 12(7), 2727–2765.
- Zhou, T., Yu, Y., Liu, Y., & Wang, B. (2014). *Flexible global ocean-atmosphere-land system model: A modeling tool for the climate change research community*. Springer.